HEAT LOSS AND HYDROTHERMAL CIRCULATION DUE TO SEA-FLOOR SPREADING

by

DAVID LEE WILLIAMS

B.A. University of Texas
(1962)

SUBMITTED IN PARTIAL FULFILLMENT OF THE
REQUIREMENTS FOR THE DEGREE OF
DOCTOR OF PHILOSOPHY

at the

MASSACHUSETTS INSTITUTE OF TECHNOLOGY

and the

WOODS HOLE OCEANOGRAPHIC INSTITUTION

June, 1974

Signature of Author.....
Joint Program in Oceanography, Massachusetts Institute of Technology - Woods Hole Oceanographic Institution, and Department of Earth and Planetary Sciences, and Department of Meteorology, Massachusetts Institute of Technology, June 1974

Certified by.....
Thesis Supervisor

Accepted by.....
Chairman, Joint Oceanography Committee in the Earth Sciences, Massachusetts Institute of Technology - Woods Hole Oceanographic Institution

HEAT LOSS AND HYDROTHERMAL CIRCULATION DUE TO SEA-FLOOR SPREADING

by

David Lee Williams

Submitted to the Massachusetts Institute of Technology - Woods Hole Oceanographic Institution Joint Program in Oceanography on May 3, 1974, in partial fulfillment of the requirements for the degree of Doctor of Philosophy.

ABSTRACT

Lithospheric cooling along the Galapagos Spreading Center at 86°W longitude, as determined by surface heat-flow measurements, appears dominated by hydrothermal circulation. This same phenomena apparently exists on the Mid-Atlantic Ridge at 36°N and presumably, in some form on all active oceanic ridges. It is responsible for removing the majority of the heat ($>80\%$) lost through young (few m.y. old) oceanic crust. This component of heat has been ignored in previous calculations of the total rate of heat loss by the Earth.

A theoretical expression is used to estimate the heat released by sea-floor spreading, since current technology does not provide any means for direct measurement. The revised value of 10.2×10^{12} cal/sec ($\pm 15\%$) represents a 32% increase over previous estimates. More than 20% of this heat apparently escapes through hydrothermal vents near sea-floor spreading centers. The previously accepted equality of oceanic and continental heat flux is invalid. The revised analysis indicates the oceanic heat flux is 2.2×10^{-6} cal/cm^2-sec (HFU) versus 1.5 HFU for the continents. The average for the Earth is then approximately 2.0 HFU.

The horizontal wavelength of inferred hydrothermal convection at the Galapagos Spreading Center, in the one dimension measured, is 6 ± 1 km. The systematic modulation suggests cellular convection. If the system is dominated by cellular convection, the depth of penetration, based on laboratory modeling experiments should be 3 to 4 kilometers.

The data from the Galapagos Spreading Center and laboratory experiments both suggest that the position of the cells in a cellular convection system can be a strong function of the local topography, the rising limbs of flow being located beneath topographic highs and the descending limbs beneath topographic lows. The addition of topography enhances the heat transfer efficiency of a convection system. Lateral variation in permeability or the systems bottom boundary condition will also influence the position of cells. Even if the circulation system were strongly influenced by some combination of variations in the strength of the heat source, topography or discrete zones of high permeability, it would probably still be cellular in nature, and similar deep penetration is indicated.

If the Galapagos Spreading Center is typical, there are presumably numerous hydrothermal springs and fissures in each square kilometer of near-ridge sea floor and sediment thicknesses of at least 50 meters are apparently penetrable to the flow of water. As the sea floor ages the surface of the hydrothermal system becomes less permeable and eventually both the surface and the deep system are completely clogged and sealed. The age at which this occurs varies from ridge to ridge but there is evidence that suggests it may not be complete until the crust is at least 8 m.y. old and possibly as much as 40-50 m.y. old. Most of the surface is apparently sealed long before hydrothermal circulation stops, although some vents do persist.

This behavior of the hydrothermal system has a dramatic effect on conductive heat-flow measurements and is largely responsible for the variations observed in conductive heat flow near active spreading ridges.

The results of this study show the difficulties in resolving systematic patterns in the heat-flow distribution on spreading ridges. Numerous, closely-spaced measurements with precise navigation combined with a relatively uniform sediment cover, appear to be necessary ingredients for recognition of the heat-flow pattern near active sea-floor spreading centers.

Thesis Supervisor: Dr. Richard P. Von Herzen
Title: Senior Scientist

ACKNOWLEDGEMENTS

I am particularly grateful for having had the opportunity to work with Dr. Richard Von Herzen. His guidance, patience, assistance and unwavering support were invaluable and will serve as an example and inspiration to me throughout my life. Dr. Robert Roy originally interested me in geothermal problems, provided help and guidance and supported me in my endeavor to shift my emphasis to marine geophysics.

Drs. Richard Von Herzen, John Sclater and Roger Anderson, after having expended great effort in gathering so much of the data contained in this thesis, willingly allowed me to work up the data and use it as my own.

Interactions with the many members of the staff and students of Woods Hole have been a great help. Jake Peirson was always ready to help me in any way he could. Drs. John Sclater, Wilfred Bryan, David Ross, Carl Bowin, John Grow and Kenneth Emery, to mention a few, always seemed interested and willing to give me a few minutes of their time.

Most of the work was supported by either the National Science Foundation Grant 16078 or through the Education Office of the Woods Hole Oceanographic Institution.

TABLE OF CONTENTS

LIST OF FIGURES

LIST OF TABLES

CHAPTER I.

INTRODUCTION

Most hypotheses treating the development of the Earth and its surface features (continental drift, sea-floor spreading, and mountain building) rely on forces resulting from the release of thermal energy within the Earth. This heat derives from many sources, most important of which are probably radioactivity and the gravitational potential energy release resulting from the formation of the Earth. The magnitude and distribution of the heat sources within the Earth are of fundamental importance in geophysics, but the only type of direct measurements that are possible are of the heat flow at the Earth's surface.

Heat is transported through the Earth by all heat transfer mechanisms (thermal conduction, radiation, and convection). The mechanism by which most heat finally escapes through the Earth's surface is thermal conduction, although I will show that convection of sea water in the oceanic crust is also quite important. In an effort to determine the magnitude and distribution of the heat conducted through the Earth's surface, numerous investigators have made several thousand geothermal heat-flow measurements both on land and on the sea floor (see Jessop et al., in press). Assuming these measurements were representative of the Earth's total heat loss, Lee and Uyeda

(1965) estimated the rate of heat loss from the Earth at 7.7×10^{12} cal/sec, based on a spatial average of conducted surface heat flow of 1.5×10^{-6} cal/cm-sec. Lee (1970) has reaffirmed this average. The distribution of heat flow is also seen to be related to the age of the crust (e.g. Langseth and Von Herzen, 1971); continental shield areas and old ocean basins characteristically display low heat flow whereas Cenozoic mountain belts and oceanic ridges generally have high heat flow.

Modern theories of sea-floor spreading hold that new oceanic lithosphere is created by the solidification and cooling of hot material as it moves away from the axis of the active oceanic ridges. Apparently sea-floor spreading is a product of deeper convective processes resulting from the Earth's inability to cool itself conductively. The earliest investigations recognized that these regions were areas of not only high, but also extremely variable, conductive heat flow (Bullard et al., 1956).

The sea-floor spreading hypothesis led to the development of several thermal models of an evolving oceanic lithosphere (Langseth et al., 1966; McKenzie, 1967; Sleep, 1969; McKenzie and Sclater, 1969; Sclater and Francheteau, 1970; and Parker

and Oldenberg, 1973). These are all conductive cooling models and, with reasonable input parameters, they all predict heat flow near the ridge axis much higher than is measured. Further, the models do not predict the scatter (Langseth and Von Herzen, 1971) or general pattern of conductive heat flow that is observed at a spreading center (Fig. 1). If the theoretical models are correct, the measured heat flux near active oceanic ridges is only a fraction of the total heat flux, consequently the Earth's rate of heat loss could be substantially higher than previously estimated. Resolving this discrepancy is of fundamental importance to the Earth scientist. This thesis investigation has its origin in an attempt to explain this phenomenon.

The pattern of conducted heat flow observed neat active oceanic ridges has been described by several authors (e.g. Talwani et al., 1971; Hyndman and Rankin, 1972; Anderson, 1972; Langseth and Von Herzen, 1971; Sclater and Klitgord, 1973). In Figure 1 I have presented several curves of heat flow versus age. All of these ridges show a general similarity. The near-axis heat flow ($<$1.5 m.y.) is relatively low. This is partially a result of biasing the observation sites in favor of sediment ponds. A maxima is observed on crust 1.5 to 3.0 m.y. old.

Figure 1. Heat flow (HFU) versus age for 8 different sections of the Earth's sea-floor spreading system. Curves are visually smoothed fits to averages taken over two m.y. intervals each one m.y. (where data is available) and projected normal to the spreading axis: (1) Galapagos Spreading Center @ 86°W Long., Sclater and Klitgord (1973), (2) Juan de Fuca Ridge, Lister (1970); (3) East Pacific Rise @ 14°S Lat.; (4) Central Indian Ocean Ridge @ 20-22°S Lat., Von Herzen and Vacquier (1966), Sclater and Harrison (1971), and Fisher, Sclater and MacKenzie (1970); (5) East Pacific Rise @ 12°S Lat.; (6) East Pacific Rise @ 39°S Lat., Erickson (personal communication); (7) Reykjanes Ridge, Talwani et al. (1971), Mid-Atlantic Ridge @ 46°N Lat., Hyndman and Rankin (1972).

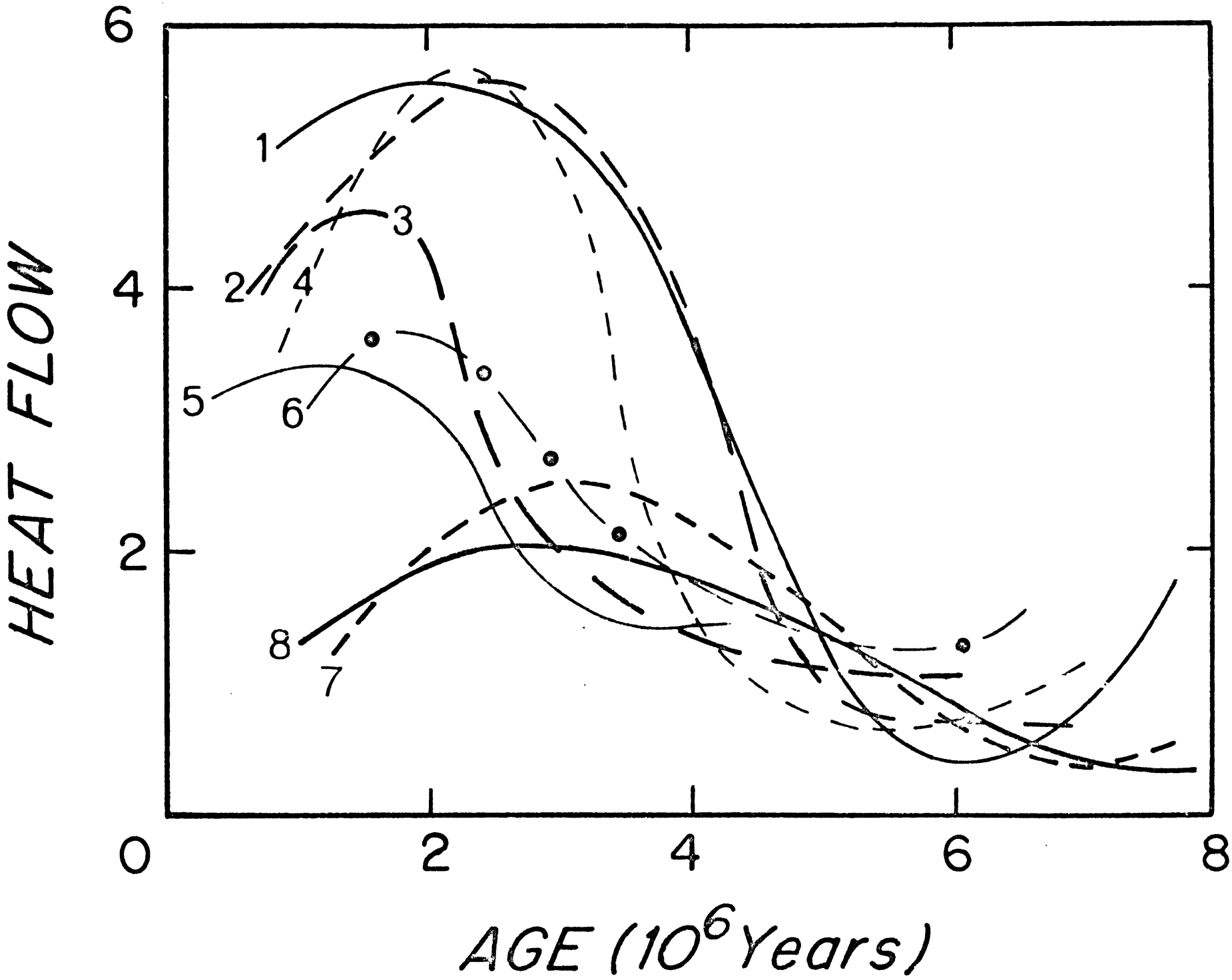
HEAT FLOW
AGE (10^6 Years)
0
2
4
6
8
1
2
3
4
5
6
7
8

This is followed by a second minima at 3.0 to 4.0 m.y. A second maxima (not shown) is freqently observed between 10 and 50 m.y. (Langseth and Von Herzen, 1971). Because the variations on the younger crust are high amplitude, short wavelength, and of presumably shallow origin, when several ridge profiles are averaged together, many of these details become less apparent. This is illustrated in Langseth and Von Herzen (1971) whose averaging technique is more suited to observing deeper phenomena.

Heat-flow observations on continental land masses, although generally time consuming and expensive, have one great advantage over oceanic observations: it is relatively simple to recognize that conduction is the dominant mechanism (Elder, 1965) by which heat passes through the surface of the continents. On the sea floor, conductive heat-flow measurements are less difficult to make but the assumption that conduction is dominant is not as well founded.

Heat-flow measurements on spreading ridges suffer from several additional limitations. First, with existing techniques, oceanic heat-flow observations are possible only in sediments, whereas active spreading centers are ideally and actually characterized by little or no sediment cover. This fact limits measurements to sea floor at least old enough to have accumulated a sufficient thickness (a few meters) of sediments.

Second, local environmental effects (e.g. rough topography, irregular sediment distribution and bottom water temperature changes) can disturb the near surface geothermal gradient (Langseth and Von Herzen, 1971; Von Herzen and Uyeda, 1963). These effects tend to be more severe near mid-ocean ridges; topographic variations are large and the sediment tends to accumulate unevenly, with greater thicknesses in the topographic lows. Finally, these techniques only measure the conductive component of the heat flux.

One explanation that has been advanced by numerous authors is that the failure of conductive-cooling models to explain the observations is due to heat loss by other heat transfer mechanisms, primarily hydrothermal convection of sea water in the crustal rocks (Elder, 1965; Palmason, 1967; Erickson and Simmons, 1969; Le Pichon and Langseth, 1969; Sleep, 1969; Deffeyes, 1970; Talwani et al., 1971; Langseth and Von Herzen, 1971; Hyndman, 1972; Lister, 1972; Anderson, 1972; Sclater and Klitgord, 1973).

Hydrothermal circulation is common in subareal volcanically active regions and extensive circulation could easily account for the discrepancy between observed and predicted heat flow. No credible arguments can be found to refute this explanation, but prior to this study very little solid evidence existed to substantiate it.

Supporting evidence for this theory is found in the hydrothermally altered rocks, e.g. serpentinite, greenstones, greenschists, and altered mineral assemblages which have been dredged from numerous sites along the Earth's oceanic spreading system (e.g. Aumento, 1971; and Miyashiro et al., 1971). Similar finds have been reported in JOIDES cores penetrating the oceanic basalt basement (e.g. Hekenian, 1974). Mineral deposits in ridge sediments and near the sediment/rock interface of JOIDES sediment cores have been attributed to hydrothermal emanations (e.g. Corliss, 1971). Extensive evidence of hydrothermal circulation has been found in ophiolitic rocks (e.g. Spooner and Fyfe, 1971) and these ophiolite suites have in turn been interpreted as uplifted oceanic crust.

Several alternative explanations have been offered for the discrepancy between conductive cooling models and observed heat flow. A good discussion of these is found in Langseth and Von Herzen (1971). However, none of these alternatives is very convincing. Most of them attribute the scatter in the data to local environmental effects. The general regional heat-flow variations, especially the zone of low flow observed on most ridge flanks, is explained by mechanisms such as endothermic phase changes, near surface mass movement from beneath the lows

toward the spreading axis, or episodic spreading. All of these processes suffer from generally reliable contrary evidence. (Sclater et al., in press; and Langseth and Von Herzen, 1971).

The first objective of this thesis study was to attempt to obtain conclusive evidence for or against the existence of substantial, deep penetrating hydrothermal circulation on an active spreading oceanic ridge.

CHAPTER II.

THE GALAPAGOS SPREADING CENTER: LITHOSPHERIC COOLING AND HYDROTHERMAL CIRCULATION

A. Background

To obtain conclusive evidence for substantial hydrothermal circulation it was necessary to make a more detailed study than had been previously attempted. The initial consideration was the choice of a ridge. Ideally the usual limitations encountered in making heat-flow measurements should be minimized. This requires qualities such as a high sedimentation rate, subdued topography, even sediment distribution and constant bottom water temperature. Next, in addition to geothermal measurements, as many as possible of the other important geological and geophysical parameters should be determined.

The Galapagos Spreading Center and the adjacent regions of the eastern equatorial Pacific have been the subject of numerous geological and geophysical studies (Herron and Heirtzler, 1967; Raff, 1968; Grim, 1970; Herron, 1972; van Andel et al., 1973; and Sclater and Klitgord, 1973). This study included a small area immediately south of the spreading center near 86°W longitude (Fig. 2), a region recently investigated in some detail by

Figure 2. Panama basin. Bathymetric contours are from van Andel *et al.* (1971) in uncorrected meters. Hatched lines mark area of detailed survey.

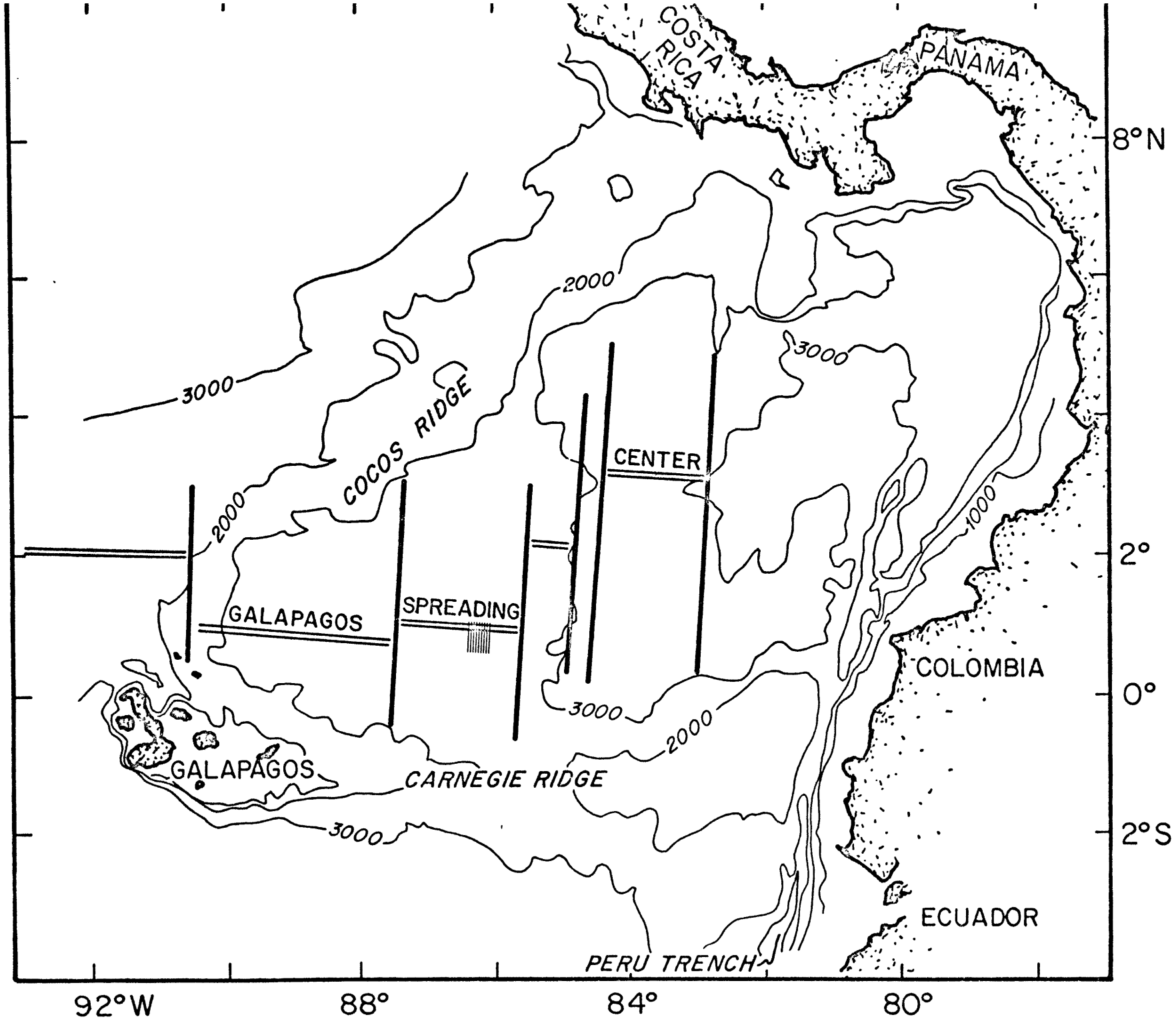
COSTA RICA
PANAMA
8°N
2000
3000
COCOS RIDGE
CENTER
2000
1000
2°
GALAPAGOS SPREADING
COLOMBIA
0°
3000
2000
GALAPAGOS
CARNEGIE RIDGE
3000
2°S
ECUADOR
PERU TRENCH
92°W
88°
84°
80°

Sclater and Klitgord (1973). The results reported here are part of a subsequent and more detailed study obtained on Legs 6 and 7 (June-August 1972) of Expedition SOUTH TOW from R/V THOMAS WASHINGTON of the Scripps Institution of Oceanography. Detailed studies of bathymetry, magnetics, sediment distribution and near-bottom water temperature structure from both surface-ship and deeply-towed instruments are described in Klitgord and Mudie (in press), and Detrick et al. (in press). In this chapter are the results of heat-flow and near-bottom water temperature measurements, and their implications for the thermal structure and the cooling of the young lithosphere of this region.

The sea floor is spreading north and south of the east-west trending spreading center located near 0°48'N latitude, at a half rate of about 34.4 mm/yr (Klitgord and Mudie, in press). This sea-floor spreading system is particularly suitable for our study because (1) the spreading history is well known, (2) the bottom topography is extremely two-dimensional and relatively subdued (Fig. 3), and (3) the sedimentation rate is high due to proximity to the equatorial high productivity belt. The latter two factors allowed heat-flow measurements to within 5 km of the spreading axis (on crust as young as 0.15 m.y.), without significant bias in the location of each station due to the local sediment distribution.

Figure 3. Bathymetry and heat flow (HFU) in survey area. Dashed lines indicate location of topographic and heat flow profiles illustrated in Figure 8. Depths are in corrected meters at a 100 meter contour interval. Heavy solid lines mark the tracks of the near bottom horizontal water temperature profiles. The circular symbols represent the location of acoustic bottom transponders.

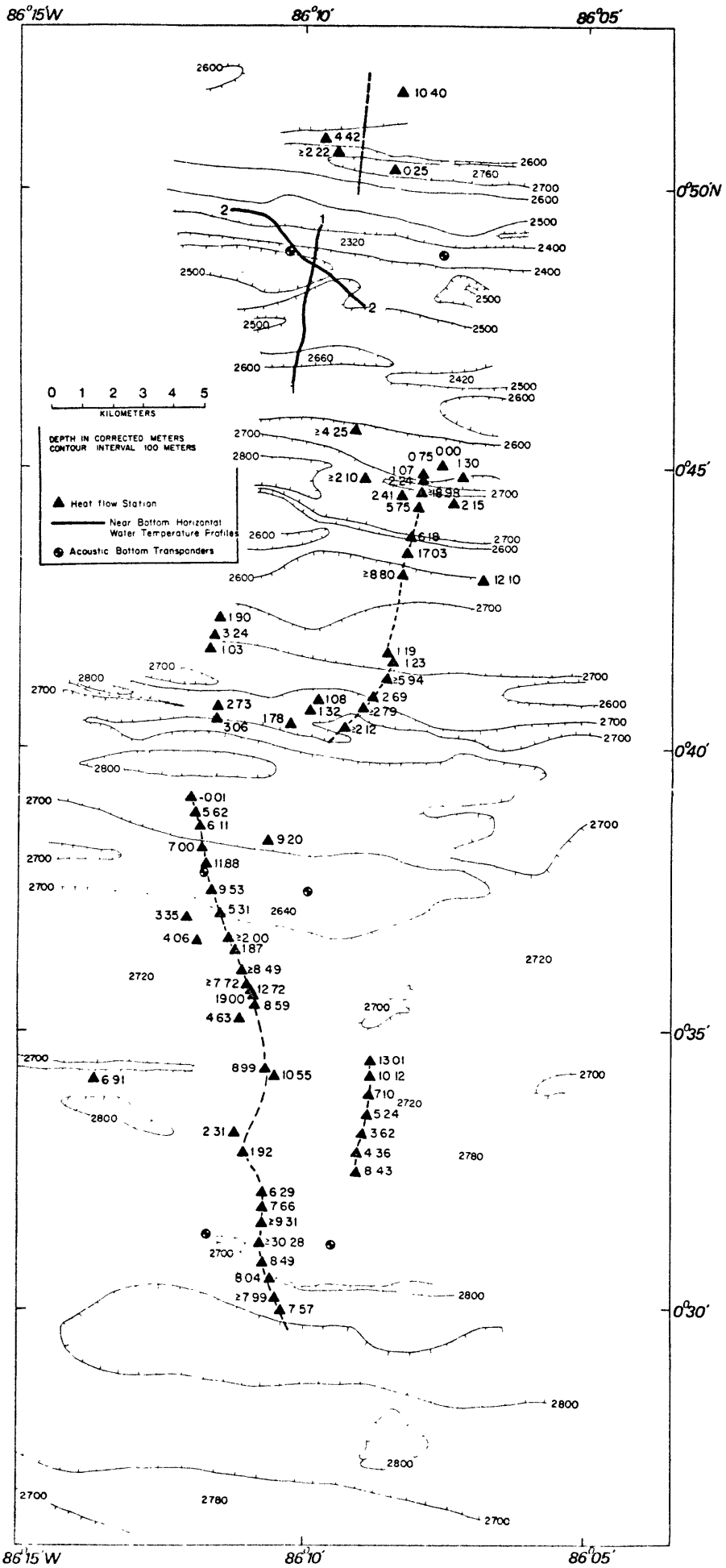
86°15'W
86°10'
86°05'
0°50'N
0°45'
0°40'
0°35'
0°30'
0 1 2 3 4 5
KILOMETERS
DEPTH IN CORRECTED METERS
CONTOUR INTERVAL 100 METERS
Heat flow Station
Near Bottom Horizontal Water Temperature Profiles
Acoustic Bottom Transponders
1
2
10 40
4 42
≥2 22
0 25
2760
2600
2700
2500
2400
2320
2660
2420
≥4 25
0 75
0 00
1 30
1 07
2 24
≥2 10
2 41
5 75
6 98
2 15
6 18
1703
≥8 80
12 10
1 90
3 24
1 03
1 19
1 23
≥5 94
2 69
≥2 79
≥2 12
1 08
1 32
2 73
3 06
1 78
-0 01
5 62
6 11
9 20
7 00
11 88
9 53
5 31
2640
3 35
4 06
≥2 00
1 87
≥8 49
≥7 72
12 72
19 00
8 59
4 63
2720
6 91
8 99
10 55
13 01
10 12
7 10
5 24
3 62
4 36
8 43
2 31
1 92
6 29
7 66
≥9 31
≥30 28
8 49
8 04
≥7 99
7 57
2780

B. Measurements and Techniques

The 71 new heat-flow measurements (Table 1) and the bottom water temperature data reported in this paper were obtained on Leg 7 of Expedition SOUTH TOW. Most of the temperature gradients in the sea floor were measured with probes designed for multiple penetrations of the sediments to depths up to 4 m, with apparatus described previously by Von Herzen and Anderson (1972) and Corry et al. (1968). Two measurements of deeper penetration (greater than 10 m) were made with thermistor probes attached to a piston corer. Thermal conductivity was determined by the needle probe method (Von Herzen and Maxwell, 1959). The thermal conductivity of our piston cores averaged 1.71×10^{-3} cal/cm-sec-°C for the upper two meters and 1.80×10^{-3} cal/cm-sec-°C on the upper four meters. These values have been assumed, as appropriate, for the other stations (Table 1). An uncertainty of ±10% in heat-flow values results from these assumptions, but this has a negligible effect for purposes of the discussion which follows.

Navigation for both the Leg 6 and Leg 7 of Expedition SOUTH TOW surveys was accomplished utilizing, whenever possible, a net of 6 acoustic bottom transponders emplaced at the beginning of the Leg 6 survey. On 12 of our heat-flow stations and

TABLE 1

Station No.	Lat. N	Long. W	Water Depth	T	P	N	K	Q
43	0°50.3'	86°8.9'	2730		2.4	3	(1.71 (0.72))	0.25 (10) i
45(1)	0°50.9'	86°10.1'	2580		2.4	3	(1.71 (0.72))	4.42 (185) i
(2)	0°50.6'	86°9.9'	2630		0.7	1	(1.71 (0.72))	⩾2.22 (⩾92)i †
46	0°51.7'	86°8.8'	2620		2.4	3	(1.71 (0.72))	10.40 (436) v
50(1)	0°45.0'	86°7.4'	2690		2.4	3	(1.71 (0.72))	0.00 (0) v
(2)	0°44.8'	86°7.1'	2700	2.06	2.4	3	(1.71 (0.72))	1.30 (55) v
51	0°43.0'	86°6.7'	2600	2.05	2.4	3	(1.71 (0.72))	12.10 (507)
52	0°44.5'	86°8.2'	2750	2.07	2.4	3	(1.71 (0.72))	2.41 (105) v
53(1)	0°45.7'	86°9.0'	2670	2.03	2.1	3	(1.71 (0.72))	⩾4.25 (⩾178) iw
(2)	0°44.9'	86°8.8'	2740	2.05	2.2	3	(1.71 (0.72))	⩾2.10 (⩾88)iw
54(1)	0°45.1'	86°7.8'	2690	2.04	2.5	3	(1.71 (0.72))	0.75±0.03 (31±1) w
(2)	0°44.9'	86°7.8'	2700	2.05	2.5	3	(1.71 (0.72))	1.07±0.03 (45±1) w
(3)	0°44.8'	86°7.8'	2680	2.04	2.9	3	(1.71 (0.72))	2.24±0.15 (94±6) w
(4)	0°44.5'	86°7.8'	2760	2.05	2.5	1	(1.71 (0.72))	⩾18.98 (⩾785) w
(5)	0°44.3'	86°7.9'	2760	2.05	2.9	3	(1.71 (0.72))	5.75±0.47 (241±20) w
(6)	0°43.8'	86°8.0'	2760	2.03	2.8	3	(1.71 (0.72))	6.18±0.48 (259±20) w
(7)	0°43.5'	86°8.0'	2590	2.03	2.5	2	(1.71 (0.72))	17.03±1.00 (715±22) w
(8)	0°43.1'	86°8.1'	2600	2.04	2.7	2	(1.71 (0.72))	⩾8.80 (⩾369) w
55(1)	0°42.2'	86°11.5'	2670		2.4	3	(1.71 (0.72))	1.90 (80)
(2)	0°42.0'	86°11.6'	2720		2.4	3	(1.71 (0.72))	3.24 (136)
(3)	0°41.7'	86°11.6'	2720	1.96	2.4	3	(1.71 (0.72))	1.03 (43)
56(1)	0°40.7'	86°11.5'	2770	2.06	2.4	3	(1.71 (0.72))	2.73 (104)
(2)	0°40.5'	86°11.5'	2730	2.06	2.4	3	(1.71 (0.72))	3.06 (128)
57(1)	0°36.6'	86°11.9'	2720		2.4	3	(1.71 (0.72))	3.35 (140) v
(2)	0°37.0'	86°12.1'	2720	2.06	2.4	3	(1.71 (0.72))	4.06 (170) v
58	0°44.3'	86°7.3'	2730	2.05	2.7	3	(1.71 (0.72))	2.15±0.16 (90±7) w
59(1)	0°41.7'	86°8.4'	2720	2.04	3.0	2	(1.71 (0.72))	1.19±0.07 (50±3) w
(2)	0°41.5'	86°8.3'	2720	2.04	2.8	2	(1.71 (0.72))	1.23±0.07 (52±3) w
(3)	0°41.2'	86°8.4'	2640	2.03	2.8	2	(1.71 (0.72))	⩾5.94 (⩾249) w
(4)	0°40.9'	86°8.7'	2680	2.04	3.0	2	(1.71 (0.72))	2.69±0.11 (113±5)w
(5)	0°40.6'	86°8.9'	2740	2.04	3.3	2	(1.71 (0.72))	⩾2.79 (⩾117) w
(6)	0°40.3'	86°9.2'	2690	2.04	3.0	2	(1.71 (0.72))	⩾2.12 (⩾89) w
60	0°38.3'	86°10.6'	2740	2.06	2.4	3	(1.71 (0.72))	9.20 (386)
61(1)	0°40.3'	86°10.2'	2740	2.06	2.4	3	(1.71 (0.72))	1.78 (75)
(2)	0°40.6'	86°9.9'	2750		2.4	3	(1.71 (0.72))	1.32 (55)
(3)	0°40.8'	86°9.6'	2730		2.4	3	(1.71 (0.72))	1.08 (45)
62	0°35.1'	86°11.1'	2720	2.04	1.*	2	1.73 (1.73)	4.63±0.45 (194±19) vw
63(1)	0°39.1'	86°12.0'	2740	2.04	2.5	3	(1.71 (0.72))	-0.01±0.03 (0±1)vw
(2)	0°38.8'	86°12.0	2720	2.04	2.9	3	(1.71 (0.72))	5.62±0.36 (236±15) w
(3)	0°38.6'	86°11.9'	2720	2.04	3.0	3	(1.71 (0.72))	6.11±0.36 (256±15) iw
(4)	0°38.2'	86°11.9'	2650	2.04	2.9	3	(1.71 (0.72))	7.00±0.22 (294±9) w
(5)	0°37.9'	86°11.8'	2640	2.03	3.0	2	(1.71 (0.72))	11.88±0.75 (497±31) w
(6)	0°37.4'	86°11.7'	2660	2.04	2.9	3	(1.71 (0.72))	9.53±0.52 (399±22) w
(7)	0°37.0'	86°11.5'	2720	2.04	2.7	3	(1.71 (0.72))	5.31±0.30 (223±13) w
(8)	0°36.3'	86°11.3'	2720	2.04	2.6	3	(1.71 (0.72))	⩾2.00 (⩾84)w
(9)	0°36.4'	86°11.3'	2720	2.03	2.7	3	(1.71 (0.72))	1.87±.06 (79±1) w
(10)	0°36.0'	86°11.1'	2720	2.04	2.8	3	(1.71 (0.72))	⩾8.49 (⩾355) w
(11)	0°35.8'	86°11.0'	2720	2.03	2.8	3	(1.71 (0.72))	⩾7.72 (⩾324) w
64(1)	0°35.7'	86°10.9'	2720		2.4	3	(1.71 (0.72))	12.72 (533) v
(2)	0°35.6'	86°10.9'	2720		2.4	3	(1.71 (0.72))	19.00 (796) v
(3)	0°35.4'	86°10.9'	2720	2.05	2.4	3	(1.71 (0.72))	8.59 (360) v
65(1)	0°34.2'	86°10.6'	2720		2.4	3	(1.71 (0.72))	8.99 (376)
(2)	0°34.1'	86°10.5'	2720	2.05	2.4	3	(1.71 (0.72))	10.55 (442)
66(1)	0°33.1'	86°11.2'	2780	2.05	2.4	3	(1.71 (0.72))	2.31 (97) i
(2)	0°32.8'	86°11.1'	2780	2.05	2.4	3	(1.71 (0.72))	1.92 (80) i
67(1)	0°34.5'	86°8.7'	2720	2.04	2.7	2	(1.71 (0.72))	13.01±0.68 (546±29) w
(2)	0°34.1'	86°8.7'	2720	2.04	2.9	2	(1.71 (0.72))	10.12±0.09 (421±46) w
(3)	0°33.7'	86°8.8'	2700	2.03	2.9	3	(1.71 (0.72))	7.10±0.44 (298±46) w
(4)	0°33.4'	86°8.8'	2730	2.04	2.8	3	(1.71 (0.72))	5.24±0.36 (215±15) iw
(5)	0°33.0'	86°8.9'	2760	2.04	2.8	3	(1.71 (0.72))	3.62±0.22 (152±9) iw
(6)	0°32.8'	86°9.0'	2780	2.04	2.7	3	(1.71 (0.72))	4.36±0.26 (183±11) iw
(7)	0°32.4'	86°9.0'	2780	2.04	2.8	3	(1.71 (0.72))	8.43±0.46 (353±19) iw
68	0°34.0'	86°13.8'	2720	2.03	11.2	5	1.78 (0.75)	6.91±0.31 (290±13) w
69(1)	0°32.0'	86°10.7'	2770	2.03	2.9	3	(1.71 (0.72))	6.29±0.17 (264±7) w
(2)	0°31.8'	86°10.7'	2750	2.03	2.9	3	(1.71 (0.72))	7.66±0.22 (322±9) w
(3)	0°31.6'	86°10.7'	2750	2.03	2.9	3	(1.71 (0.72))	⩾9.31 (⩾390) w
(4)	0°31.1'	86°10.7'	2730	2.03	2.1	2	(1.71 (0.72))	⩾30.28 (⩾1270) w
(5)	0°30.8'	86°10.7'	2750	2.04	2.9	3	(1.71 (0.72))	8.49±0.46 (356±19) w
(6)	0°30.5'	86°10.6'	2790	2.04	2.9	3	(1.71 (0.72))	8.04±0.44 (337±18) w
(7)	0°30.2'	86°10.5'	2760	2.04	2.8	3	(1.71 (0.72))	⩾7.99 (⩾334) w
(8)	0°29.9'	86°10.4'	2780	2.04	2.9	3	(1.71 (0.72))	7.57±0.22 (318±9) w

TABLE 1 CAPTION

T is bottom water temperature (°C).

P is the estimated sediment penetration (m) of lowermost probe used for temperature gradient measurements.

N is number of thermistors used for sediment temperature gradient measurements.

K is the thermal conductivity in 10^{-3} cal/°C-cm-sec (W/m-°k). Outer parenthesis indicate values assumed from measurements on nearby piston cores.

Q is heat flow in 10^{-6} cal/cm^2 sec (10^{-3} W/m^2). Measurements made by Woods Hole Oceanographic Institution are indicated by a with values and probable errors of these computed as in Von Herzen and Anderson (1972). Unless otherwise annotated, minimum values result from a tilt greater than our instruments can measure ($\geqslant$ 30 degrees off vertical). i, v represent measurements in which the instrument or vessel respectively were acoustically navigated.

* Station 62 - some penetration beyond 10 m was indicated. The difficulty of fixing the actual penetration depth is discussed in the text.

† Only one thermistor on scale.

Water depth in corrected meters.

both of the near-bottom horizontal water temperature profiles, the instrumentation was navigated inside the transponder net with near-bottom acoustic equipment attached to the hoisting cable (Boegeman et al., 1971); the positioning had an accuracy of ±200 meters relative to the bathymetry (Fig. 3). On an additional 10 heat-flow stations it was possible to navigate the ship only acoustically. The position of the heat-flow measurement was determined from an empirical relation between wire angle and horizontal distance to the relay transponder on stations where relay transponder navigation was available. We estimate the uncertainty of station positions determined by this method at ±400 meters. No acoustic navigation was available for the remaining 48 heat-flow stations. These stations were located by a combination of satellite navigation, bathymetry (Klitgord and Mudie, in preparation), ranges to a single bottom transponder, and computer-generated dead reckoning. The quality of these positions varies appreciably but the average is probably no better than ±1 km. Our ability to locate all our stations is somewhat better in latitude than longitude due to the east-west grain of the bottom topography. On most stations multiple penetrations were made. The relative positions between individual measurements on these stations are generally determined better than ±300 meters.

As many as 11 heat-flow measurements over horizontal distance of greater than 7 km were made during a single station with the multipenetration probe described in Von Herzen and Anderson (1972).

In addition to our heat-flow measurements, two near-bottom horizontal water temperature profiles were obtained utilizing the apparatus depicted in Figure 4. The lower thermistor was generally maintained within 10 meters of the sea floor. The temperature of each of the lower two thermistors was recorded twice every 30 seconds at different sensitivities. The upper thermistor temperature was recorded at high sensitivity once every 30 seconds. The potential temperatures have a precision of about ±0.003°C at high sensitivity and ±0.015°C at low sensitivity. Only the high sensitivity records are plotted in Figure 9.

C. Observations

A synthesis of the heat-flow and water temperature data (Figs. 3, 6, 7, 8, and 9) lead to the following observations: (1) conductive heat-flow measurements vary regularly from relatively low values averaging about 2×10^{-6} cal/cm^2-sec (HFU) to high values averaging about 12 HFU, with extremes of individual measurements ranging from zero to greater than 30 HFU.

Figure 4. Apparatus used in measuring horizontal water temperature profiles. Altitude above the bottom was maintained by echo sounding from the telemeter.

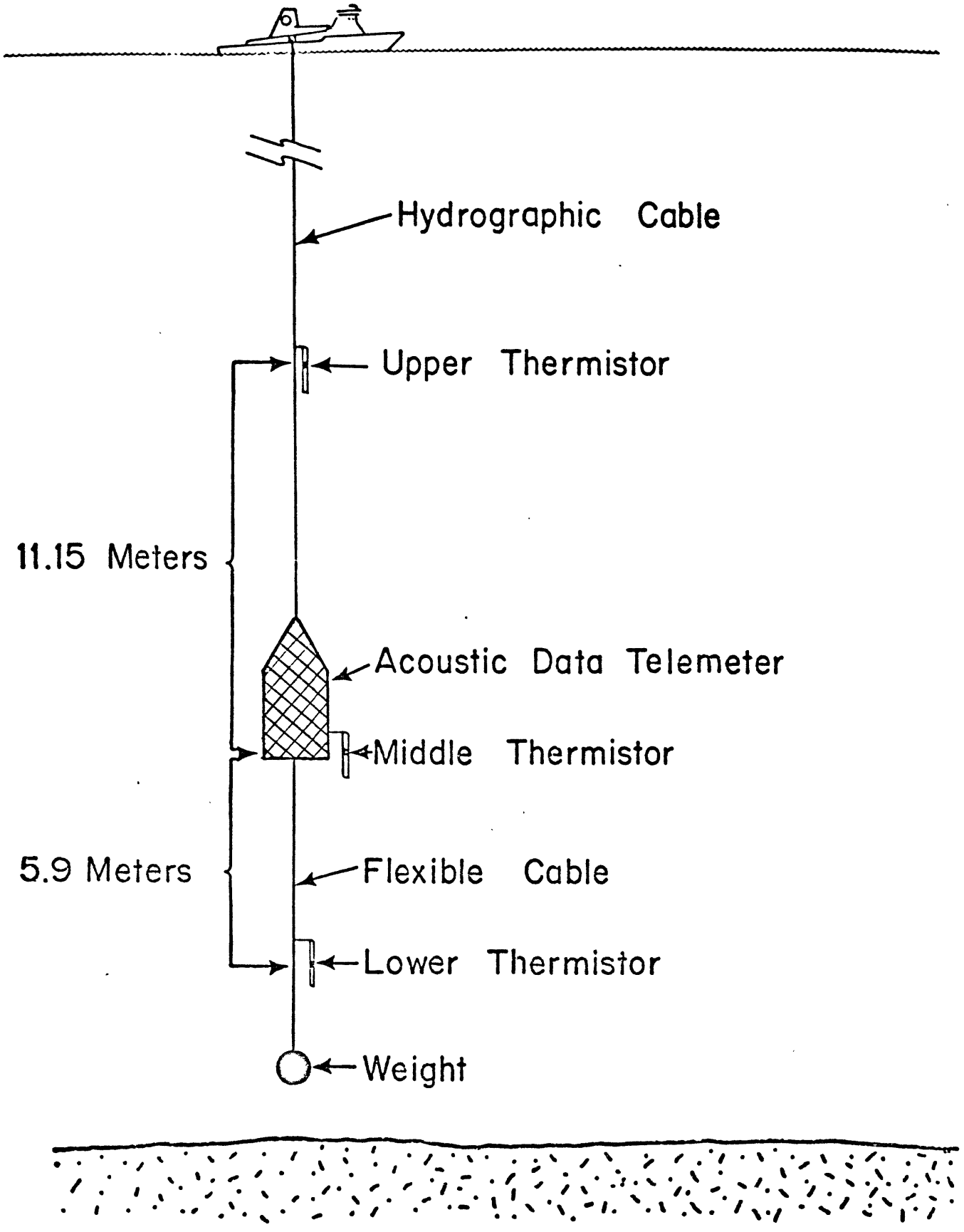
Hydrographic Cable
Upper Thermistor
11.15 Meters
Acoustic Data Telemeter
Middle Thermistor
5.9 Meters
Flexible Cable
Lower Thermistor
Weight

A significant north-south variation in heat flow exists with a modulation wavelength of approximately 6 ±1 km (Fig. 6). It is clear from a close examination of Figure 6, and particularly from the individual profiles in Figure 7, that the heat-flow pattern is complicated. However, heat-flow maxima are marked by an absence of low values, and the heat-flow minima are almost as well defined. (2) The average heat flow gradually increases with distance south of the ridge axis, whereas the theoretical heat flow, based on conductive cooling models (McKenzie, 1967; Sclater and Francheteau, 1970), decreases rapidly with distance from the axis (Fig. 6). (3) Near the spreading center the average of the measured values is much less than the theoretical value but at the southern end of our survey this average clearly approaches the theoretical curve (Fig. 6). (4) The heat-flow minima tend to be on or near topographic lows and the heat-flow maxima are associated with either scarps, topographic highs, or fields of mounds (Figs. 6, 7, and 8). The mounds are found only in the southern half of our area and average about 5-10 m high with a 25 m radius, as determined from deep-tow echo sounding and side-looking sonar (Klitgord and Mudie, in press). (5) On station 62 (Fig. 11) the observed thermal gradient extrapolated to the bottom water temperature yields an apparent penetration

of 18.3 m for our 10-m piston core. Although there were other indications of some superpenetration, 8.3 m seems unlikely. (6) The average of all our measured heat-flow values is greater than 5.9 HFU. This is in good agreement with Sclater and Klitgord (1973). It is much higher than the world-wide average of conductive heat flow (1.5 HFU, Lee, 1970). It is also significantly higher than has been measured at other spreading centers on crust of similar age (Langseth and Von Herzen, 1971). (7) Several significant bottom water temperature anomalies can be seen in Figure 9. The largest temperature anomaly is observed over the regional topographic high, an east-west ridge located at 0°49'N latitude. This ridge apparently represents a boundary between different water types above and below the ridge crest, as observed by Sclater and Klitgord (1973) and Detrick et al., (in press). The other water temperature anomalies cannot be explained by bottom temperature structure or currents. Anomalies located at 2.76, 3.26, and 4.80 km along our track are significantly above the noise level of our measurements and appear on more than one sensor.

Figure 5. Sketches illustrating the effect of hydrothermal circulation on geothermal gradients measured at the sea floor. Heavy solid lines represent isotherms and dashed lines with arrows show the general pattern of convection. (a) Convection in crustal rocks below an impermeable sediment blanket. (b) Convection which penetrates the sediment cover allowing for exchange with the bottom waters. The effect on the conductive heat flow pattern is shown above each sketch.

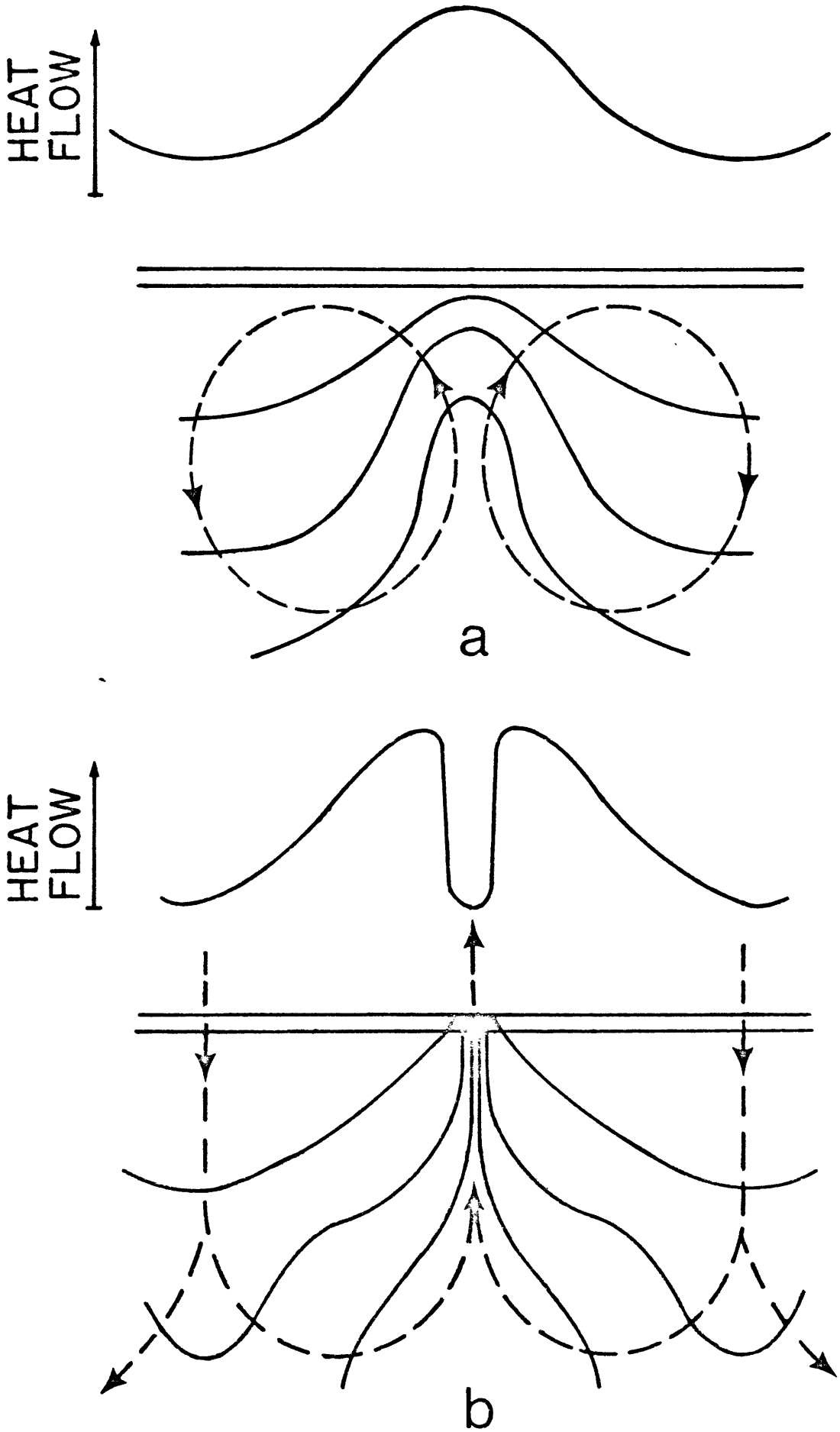
HEAT
FLOW
a
HEAT
FLOW
b

Figure 6. Heat flow data, topography and sediment thickness (stippled pattern) from the 4 profiles shown by dashed lines in Figure 3 (projected north-south). The vertical exaggeration is 12.5:1. Closed circles are individual heat flow values which were within 2 km of profile. Crosses represent depth of heat flow measurements deviating 20 meters or more from the plotted topography. Triangles indicate minimum values of heat flow. Open circles and triangles represent heat flow stations more than 2 km away from the profile track. The circle with a cross in it is station 62. It is discussed in the text and is not used in the averages. The dashed line is the theoretical heat flow (from Sclater and Francheteau, 1970) for an 85 km thick lithosphere, 1250°C on its lower boundary, an internal heat generation of 2.0×10^{-14} cal/cm^3-sec and an average thermal conductivity of 6.9×10^{-3} cal/cm-sec°C. The solid lines connect averages of the measured heat flow values (vertical bars are ± standard error) averaged over two kilometer intervals every one kilometer along a profile.

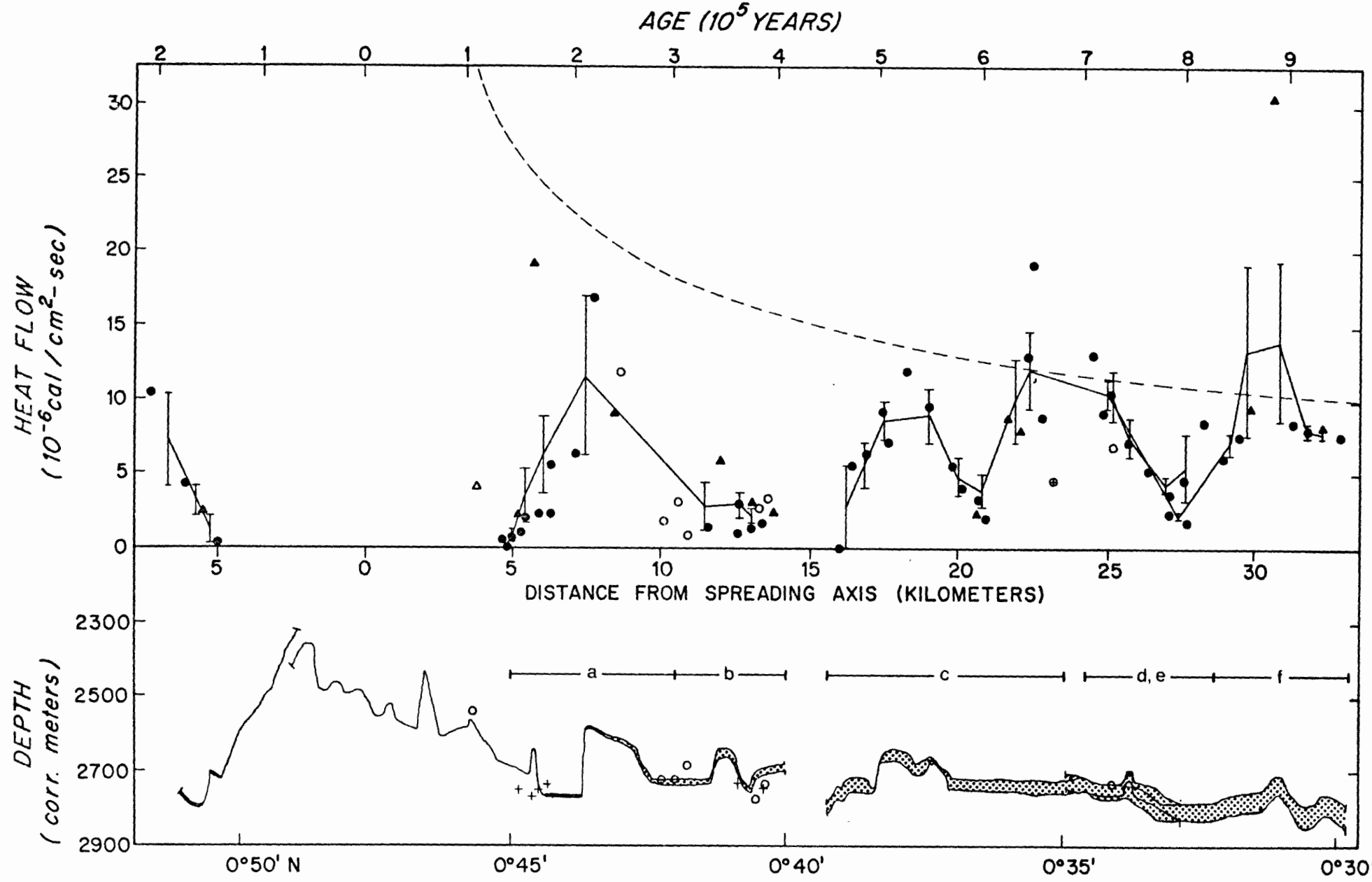
AGE (10^5 YEARS)
2 1 0 1 2 3 4 5 6 7 8 9
HEAT FLOW (10^{-6}cal/cm^2-sec)
30 25 20 15 10 5 0
5 0 5 10 15 20 25 30
DISTANCE FROM SPREADING AXIS (KILOMETERS)
DEPTH (corr. meters)
2300 2500 2700 2900
a b c d, e f
0°50' N 0°45' 0°40' 0°35' 0°30'

Figure 7. Sediment and basement bathymetry from Klitgord and Mudie (in press). Each bathymetric profile is from an S.I.O. deep-tow instrument package survey line that passes near the heat-flow station. The position of each profile is shown in Figure 6. The location of mounds refers to the fields of sediment mounds discussed in the text. In general these mounds are too small to be seen at the vertical scale used in the figure. Numbers above the arrows are heat-flow values in 10^{-6} cal/cm^2 sec. Depths are in corrected meters with a vertical exaggeration of 4:1. Since the heat-flow stations were not located exactly on the bathymetric survey lines the relative geographical positions of the heat-flow stations have been adjusted to best reflect the actual bathymetry at the site of the heat-flow station. Only heat-flow measurements near each bathymetric profile are shown. As a result not all our measurements are illustrated.

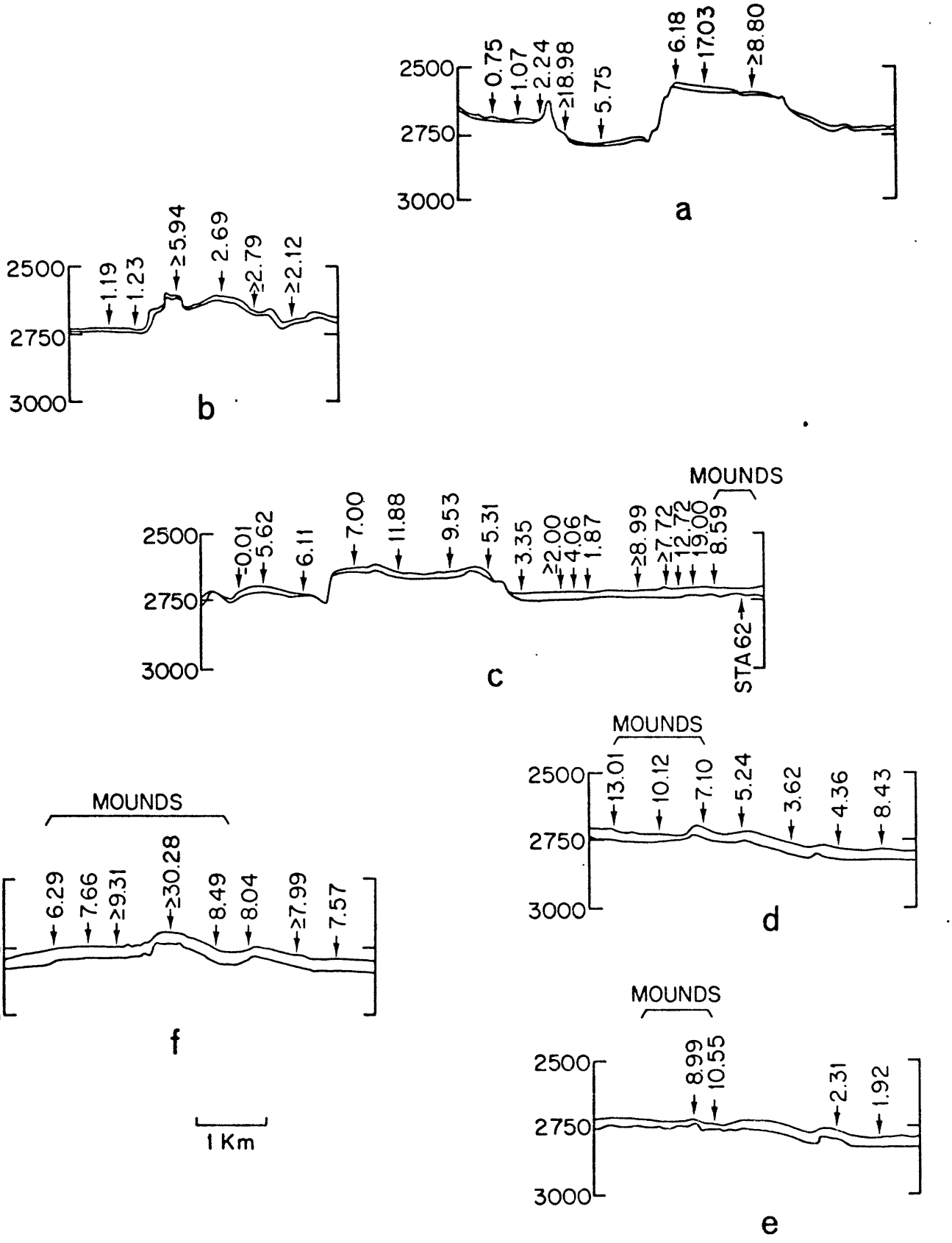
2500
2750
3000
0.75
1.07
2.24
≥18.98
5.75
6.18
17.03
≥8.80
a
1.19
1.23
≥5.94
2.69
≥2.79
≥2.12
b
MOUNDS
-0.01
5.62
6.11
7.00
11.88
9.53
5.31
3.35
≥2.00
4.06
1.87
≥8.99
≥7.72
12.72
19.00
8.59
STA 62
c
MOUNDS
13.01
10.12
7.10
5.24
3.62
4.36
8.43
d
MOUNDS
6.29
7.66
≥9.31
≥30.28
8.49
8.04
≥7.99
7.57
f
1 Km
MOUNDS
8.99
10.55
2.31
1.92
e

Figure 8. A sketch map of our survey area. The heavy east-west trending dark lines mark the positions of fault scarps identified by Klitgord and Mudie (in press). If these faults are zones of high permeability they could be important in the hydrothermal system. The small dots represent the general location of sediment mounds. Note the correlation of these mounds with areas of high heat flow.

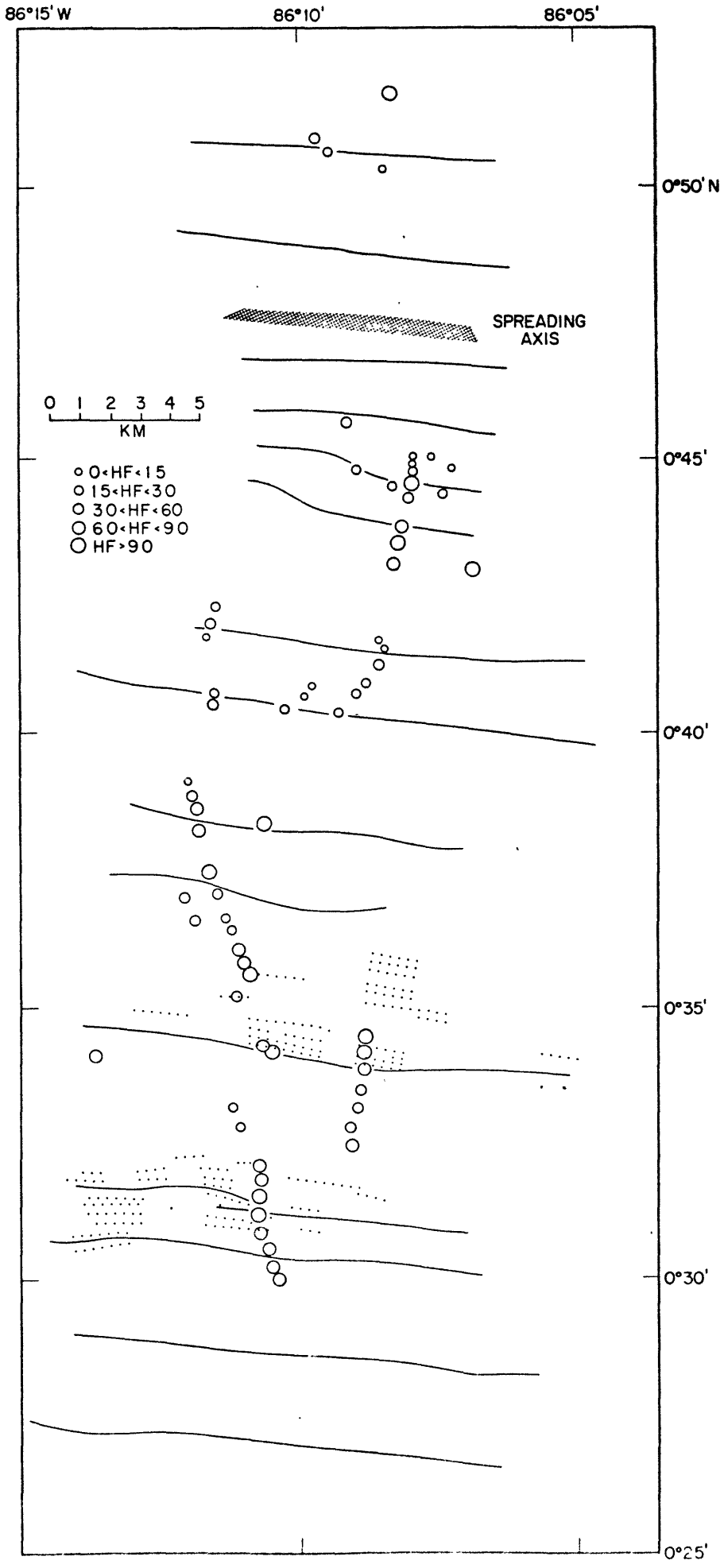
86°15' W
86°10'
86°05'
0°50' N
0°45'
0°40'
0°35'
0°30'
0°25'
SPREADING AXIS
0 1 2 3 4 5
KM
0<HF<15
15<HF<30
30<HF<60
60<HF<90
HF>90

Figure 9. Bottom water horizontal temperature profile, No. 1. U + 0.05°C is the potential temperature of the upper thermistor plus 0.05°C. M is the potential temperature of the middle thermistor and U -0.05°C is the lower thermistor potential temperature minus 0.05°C. The average horizontal speed was 1.28 km/hr. The thermistor depth trace shows much more roughness than the bottom because it is derived by subtracting a detailed thermistor altitude signal from less detailed bottom depth data. Therefore, much of the roughness in the thermistor depth is actually roughness of the bottom.

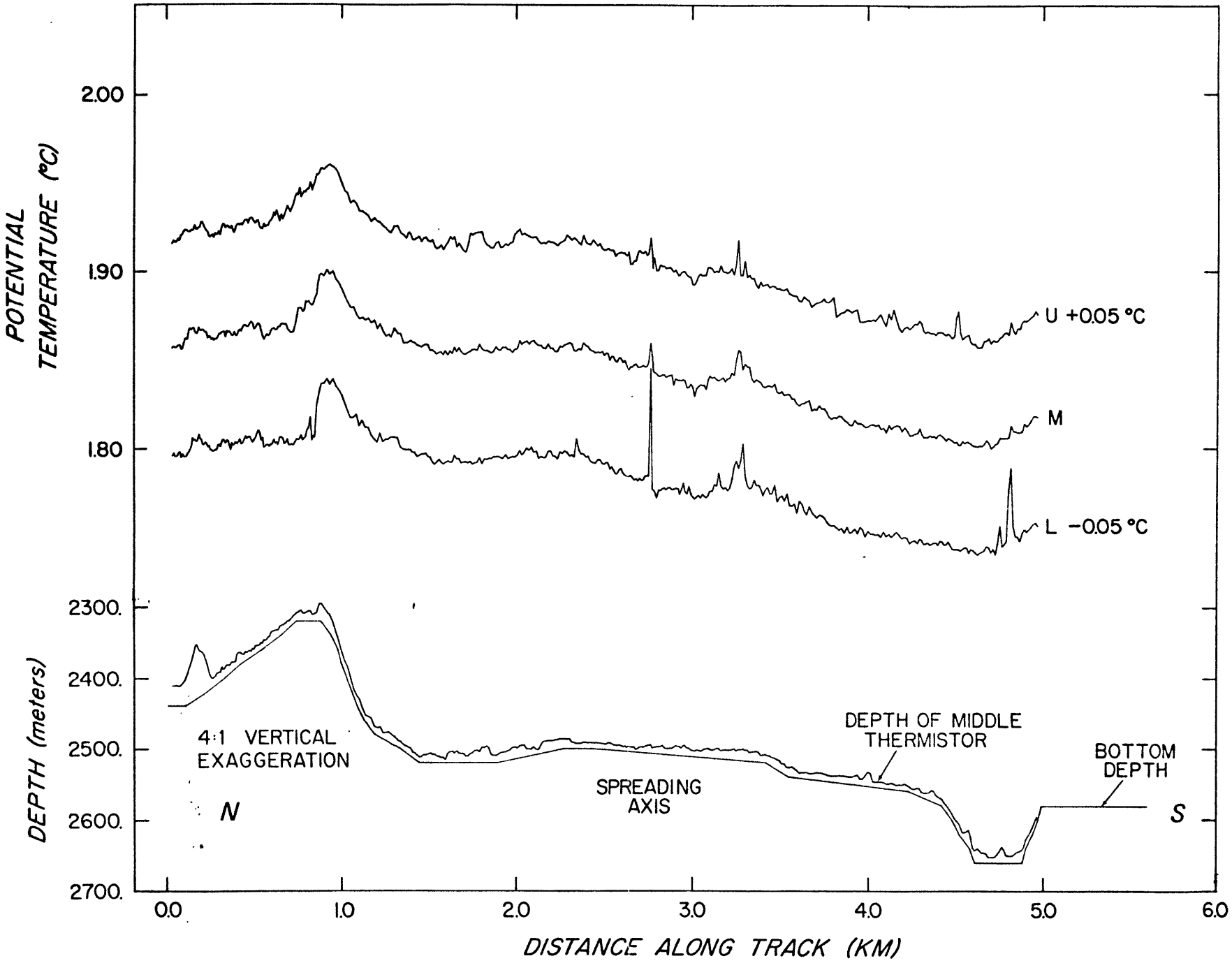
POTENTIAL TEMPERATURE (°C)
2.00
1.90
1.80
U +0.05 °C
M
L −0.05 °C
DEPTH (meters)
2300.
2400.
2500.
2600.
2700.
4:1 VERTICAL EXAGGERATION
N
SPREADING AXIS
DEPTH OF MIDDLE THERMISTOR
BOTTOM DEPTH
S
0.0
1.0
2.0
3.0
4.0
5.0
6.0
DISTANCE ALONG TRACK (KM)

D. Interpretation

D.1. Conductive heat-flow measurements in a hydrothermal area

(a) General. Since we will use hydrothermal circulation to explain our observations it is worthwhile to discuss what we should expect from conductive heat-flow measurements in a hydrothermal area. Thermal gradients can be radically distorted by hydrothermal circulation. The sketches in Figure 5 illustrate the effect of a hypothesized water circulation pattern on subsurface isotherms. When the circulating system is confined to permeable rock which is overlain by an impermeable sediment cap (Fig. 5a), larger thermal gradients will be measured above the rising limbs than above descending limbs. Thermal gradients should grade evenly between the limbs. But if the circulating system has free discharge and re-charge (Fig. 5b) thermal gradients near the axis of both rising and descending limbs can be quite small. In this case, since the sediment temperatures near the rising limb are much higher, it is still possible to separate these two causes. The pattern of heat flow between the limbs depends on the character of the system but we should find a heat-flow maximum adjacent to the discharge vent. More generally, the net effect of hydrothermal waters venting through the sea floor is to lower the regional geothermal gradient.

(b) Heat-flow minima. Since the Galapagos Spreading Center appears to be actively spreading and thus is a volcanically active region, high temperature rock and magma can be expected near the surface. If conduction is the dominant heat transfer mechanism, we should find a consistently high geothermal gradient, instead we find regularly spaced minima. Occasional low gradients might be produced by sediment slumping (Von Herzen and Uyeda, 1963) but the sediment distribution on the spreading center is fairly uniform. Most steep basement slopes (fault scarps) tend to have thinner sediment cover, as expected; the thin cover also extends to the base of these slopes, suggesting that these may be active fault scarps and that sediment slumping is minimal. Corrections for the effects of topography (e.g. Lachenbruch, 1968), although small, would generally tend to accentuate the observed modulation. Similarly, thermal refraction caused by the conductivity contrast between rock and sediment is small because of the uniform sediment cover. These corrections were derived for regions in which thermal conduction is dominant and it would be inappropriate to apply them if thermal convection might be important. Therefore, no attempt has been made to modify our heat-flow values for these effects. We have seen no evidence in the bottom sediment gradients for

significant temporal changes in bottom water temperature. Small variations in the temperature of the bottom water with periods shorter than a few days or longer than a few years might be difficult to detect but would not significantly affect our discussion.

The pattern of heat-flow variations, and the lack of evidence for other causes, seems to require hydrothermal circulation of sea water in the crustal rocks. Lacking any high sediment temperatures that could mark a hydrothermal vent, we conclude that the areas of low heat flow represent either (1) regions where the sea water is entering the crustal rocks, if the upper boundary of the system is still open, or (2) areas above the downgoing limb of a closed convective system.

(c) Magnitude of hydrothermal cooling. Using the same theoretical heat-flow model illustrated in Figure 6 (Sclater and Francheteau, 1970, eqn. 23), lithospheric creation along the Galapagos Spreading Center results in a continuous heat loss of 1100 cal/sec per centimeter of ridge length. Of this total more than 330 cal/sec-cm is released through crust less than 35 km from the axis. This is a minimum value because it is based on a conductive cooling model, and the combination of conduction and hydrothermal convection would remove heat more efficiently.

The heat loss that would result if the upper 500 meters of the crust were produced by extrusive lavas would account for only about 15 cal/sec-cm. In this calculation we assume the lava is solidified causing each gram to release 100 cal of latent heat and then cooled from 1250°C to 0°C which releases an additional 300 cal of sensible heat. The average of our conductive heat-flow measurements within 35 km of the axis gives 36 cal/sec per centimeter of ridge length. This implies that more than 80% of the geothermal heat released in our survey area escapes through hydrothermal vents.

(d) Heat flow vs. age. The increase of conductive heat flow southwards from the spreading center (Fig. 6) suggests that the free exchange of water and therefore the magnitude of the hydrothermal component of heat loss decreases as sediment accumulates. Only after the sediment blanket is sufficiently thick that it begins to form an impermeable cap, as is apparently the case near the southern end of our survey, does thermal conduction become the dominant heat transfer mode at the sediment/water interface. The permeability of these ridge sediments is not known, but they apparently remain significantly penetratable for fluid flow to thicknesses of at least 50 meters.

Increasing heat flux with age has been observed on other active ridges (Talwani et al., 1971; Hyndman and Rankin, 1972). However, on the Galapagos Spreading Center the measured heat flow approaches the theoretical value at a younger age. This is probably a result of the higher sedimentation rates and smoother topography, causing the upper boundary of the hydrothermal system to be sealed more quickly.

The observed thermal gradients imply the existence of large horizontal temperature variations and, furthermore, that the average temperature of near surface rocks increases with age. This is contrary to what one might normally expect from a simple model.

(e) Effect of hydrothermal circulation on crestal topography. The crestal zone of the Galapagos Spreading Center is dominated by faulted blocks tilted outward with scarps facing the crest (Fig. 10)(Klitgord and Mudie, in press). Scarps on blocks 0.25 million years old are offset (ΔH) an average of about 100 meters, whereas those in 1.0 million years old crust have a ΔH of only 50 meters. Further, during this same period, the blocks increase in depth from approximately 2600 meters to 2700 meters.

Figure 10. Schematic representation of crestal block faulted topography. The average depth of each block increases with age whereas the scarp offset (ΔH) decreases. Dashed line indicates horizontal reference level.

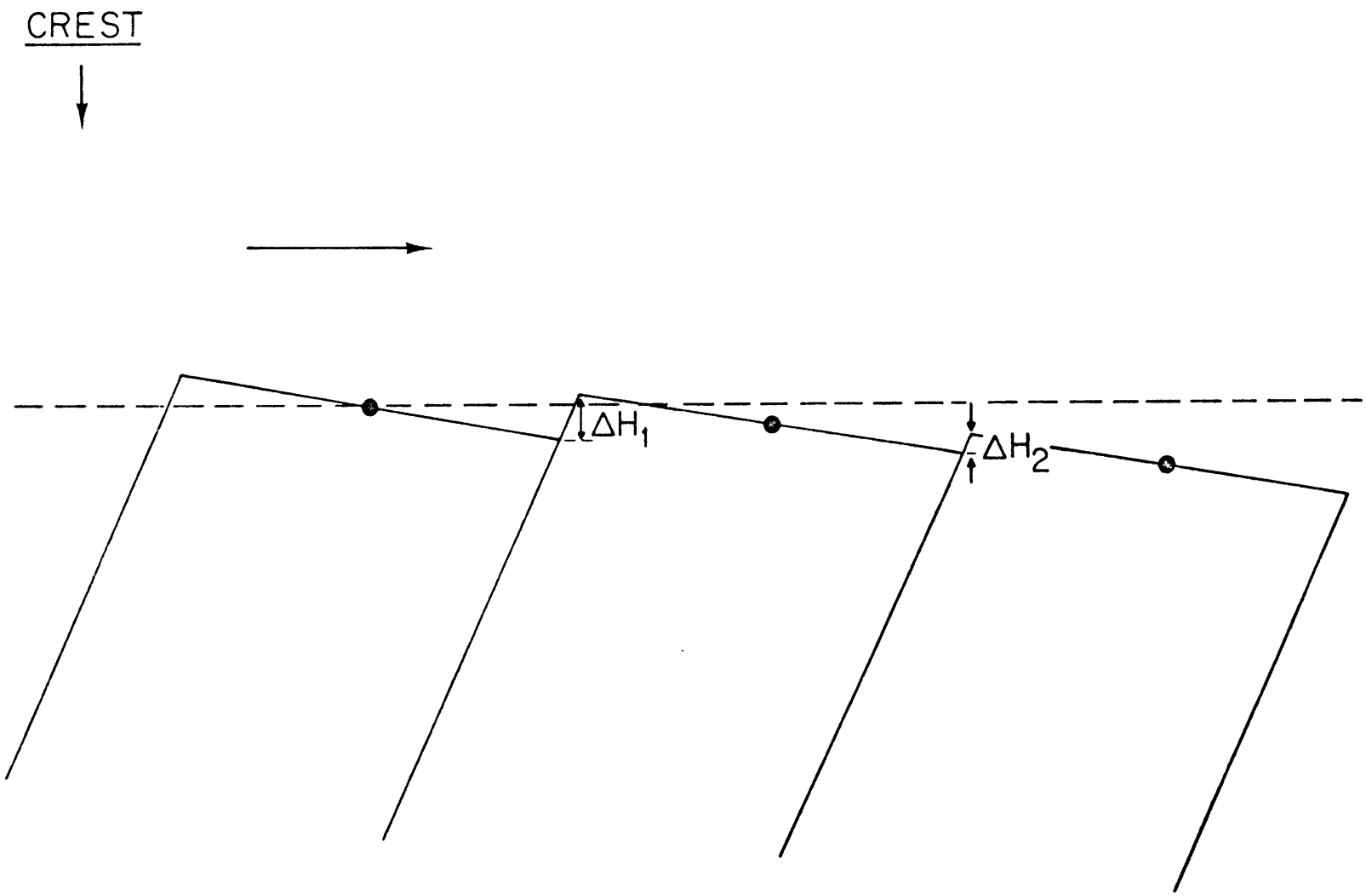
CREST
ΔH1
ΔH2

Classical thermal contraction (Sclater and Francheteau, 1970), lithospheric thickening (Williams and Poehls, in prep.) and the relaxation of dynamic uplift (Lachenbruch, 1973) all predict this general decrease in elevation as the young crust ages.

Hydrothermal circulation provides us with an additional mechanism for generation of the crustal elevation changes. Circulation of sea water in the crustal blocks produce hydration of the oceanic crust. As the crustal blocks spread from the intrusion zone, portions of the blocks are reheated from below. This can produce metamorphic upgrading of the hydrous assemblage which may account for an additional overall elevation decrease. In general, low-grade metamorphic rocks have larger volume changes (Δv) of reaction than higher grade metamorphic rocks. This can be demonstrated by comparing volume changes from the upgrading of prehnite + chlorite + quartz to epidote + tremolite + water. This is a typical active ridge metamorphic suite and reaction produces a volume change of -4% (Table II), at STP. Thermal expansion and compressibility coefficients for these universals are unknown but the low pressures and temperatures involved should make the STP calculation accurate to within ±10%.

Thus, if the hydrated crustal blocks are 5 km thick, less than 50% of the crust undergoing this reaction would produce

TABLE II

Standard temperature and pressure, molar volumes for the reaction:

Prehnite + Chlorite + Quartz $\rightleftharpoons$ Epidote (Zoisite) + Tremolite + Water

$$5\ Ca_2Al_2Si_3O_{10}(OH)_2 + Mg_5Al_2Si_3O_{10}(OH)8 + 2SiO_2 \rightleftharpoons 4Ca_2Al_3Si_3O_{12}(OH) + Ca_2Mg_5Si_8O_{22}(OH)_2 + 6H_2O$$

Component	Volume (cm^3/mole)
Prehnite	142.20 +++
Chlorite	213.01 ++
Quartz	22.69 +
Eqidote (Zoisite)	136.50 +
Tremolite	272.95 +
Water	18.07 +

Volume change of solids for the reaction * = -42.05

---

* All volumes treated as constants.

+ From Robie et al., 1966.

++ Calculated from unit-cell dimensions of prochlorite from Steinfink, 1958, 1961, 1962a.

+++ Calculated from unit-cell dimensions from Preisinger, 1965.

the entire observed elevation decrease assuming that all of the volume change goes into elevation change. Similarly, the scarp offsets may be maintained to some extent by the existence of large horizontal temperature differences within blocks and between adjacent blocks. We would expect the offset to be reduced as the crust ages and these temperature differences decrease. It is clear that hydrothermal circulation and the resulting chemical alterations can have a substantial effect on crestal topography. Until we have a better understanding of the thermal, petrologic and chemical properties of the oceanic lithosphere it will be difficult to separate these effects from those of classical thermal contraction, lithospheric thickening and dynamic uplift in controlling crestal topography.

(f) Geographic distribution and magnitude of heat flow.

The geographical distribution of our data is insufficient to determine whether the observed variations in heat flow largely are two-dimensional, like the topography, or three-dimensional. Furthermore, a theoretical model with inherent uncertainties is required to estimate the magnitude of heat released by hydrothermal circulation on the spreading center. We can only say that this circulation appears to control the near-axis conductive heat-flow pattern and that this pattern bears only a limited

relationship to the actual heat flux. In regions where the hydrothermal system still has a free exchange with the bottom water, the theoretical models provide a more realistic means to estimate the heat flux than the measured values of conductive heat flow. Even where the sediment forms an impermeable upper layer, hydrothermal circulation may persist in the crustal rocks below the sediment, which clearly requires a large number of measurements spaced significantly closer than the scale of the circulation pattern to obtain a reliable value of the regional heat flux.

D.2. Character of the hydrothermal system

(a) Hydrothermal vents. Reasonably clear evidence for hydrothermal vents is presented from the bottom water temperature anomalies of Figure 9. With expressions developed empirically by Rouse et al. (1952), and discussed by Batchelor (1954) and Turner (1969), it is possible to make a rough estimate of the heat transfer by steady-state thermal plumes of this size. The rate of heat loss F represented by a two-dimensional plume is

$$F = \left[\frac{zg'}{2.6} \exp(41x^2/z^2)\right]^{3/2} \text{ cal/sec-cm}$$

and for a three-dimensional plume

$$F = \left[\frac{z^{5/3}g'}{11} \exp(71r^2/z^2)\right]^{3/2} \text{ cal/sec}$$

where $g' = \alpha g(T-T_o)$ with g the gravitational acceleration and T the anomalous temperature observed at distance z above the bottom and at distance x or radius r from the vertical axis of the plume. The coefficient of thermal expansion α is taken for the fluid medium at ambient temperature T_o. These equations assume that the composition of the plume water is not significantly different than the bottom water, that the plume is from a point or line source, and that it is not significantly affected by bottom currents.

We estimate the anomaly near 2.76 km in Figure 9 at 1600 ±300 cal/sec for a three-dimensional plume or 13.4 ±3.6 cal/sec-cm for a two-dimensional plume. The uncertainties derive from those associated with the temperature data. We have assumed that profile was directly above the source, so that the values of F should be considered minimal.

Extrusive lava flows can be expected to heat the water that quenches and cools them. However, in an area as small as the one covered by our water temperature profile lava flows should be very infrequent with the lava cooling quickly. Therefore, we feel that the observed temperature anomalies are more probably caused by thermal plumes rising from hydrothermal vents.

The correlation between heat-flow maxima and the occurrence of small sediment mounds (Fig. 6 and 7d, e and f) suggests that these mounds are hydrothermal vents. They seem to have no expression in the basement topography and they tend to be lineated as though they were above a hydrothermal fissure in the basement rock (Klitgord and Mudie, in press). We can only speculate about the character of the flow from these vents. It could be continuous or periodic. The fact that these mounds appear only in areas of high heat flow implies the elements of the hydrothermal system remain nearly fixed with respect to the underlying crust for long periods of time. At the observed sedimentation rates, it would take more than one hundred thousand years to bury one of these mounds after it became inactive. Interestingly, our station 62 has combined the qualities of a relatively low thermal gradient and high sediment temperatures (Fig. 11) expected of a measurement near an active hydrothermal vent (Fig. 5b) and is located within one of these fields of sediment mounds. This explanation of the unusual temperature-depth relation seen in Figure 11 may be more probable than excessive superpenetration of the coring apparatus.

Figure 11. Relative temperature versus depth for station 62. Depths are from the bottom of the piston corer weight stand. Any amount of superpenetration would increase these depths. Temperatures are relative to the bottom water temperature (2.04°C ±.01°C). There were four thermistors mounted on the core barrel. The lower two, whose position are indicated by arrows, were sensing relative temperatures which were greater than 3.9°C, the highest our instrumentation was set to record.

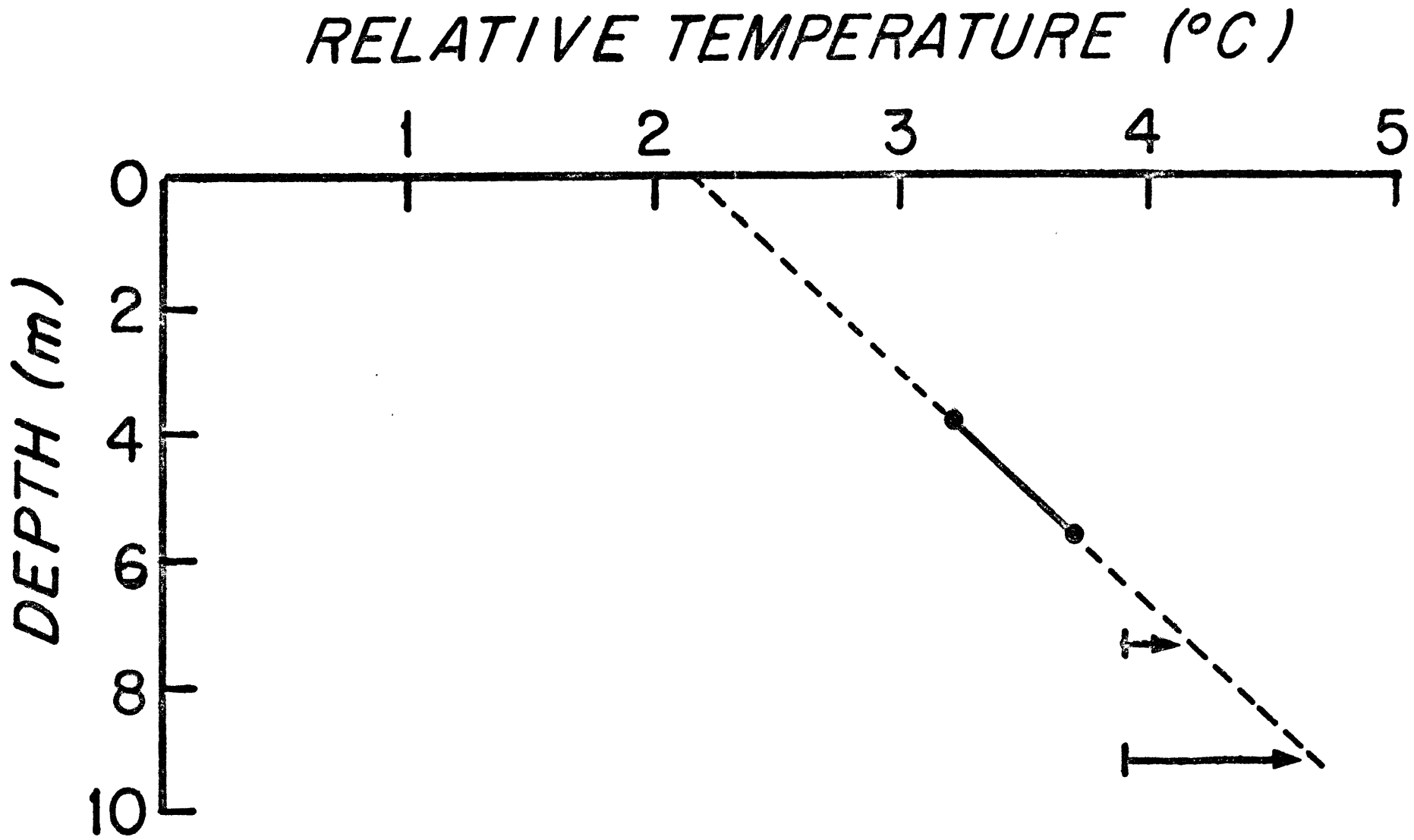
RELATIVE TEMPERATURE (°C)
1
2
3
4
5
DEPTH (m)
0
2
4
6
8
10

The heat transfers we have calculated for some of the plumes, deduced from Figure 9, represent a significant percentage of the total regional heat loss. Yet, just a few meters above the bottom, the predicted and observed temperature anomalies are less than 0.1°C. Larger temperature anomalies would be expected closer to the vent. Also if the vented water were warmer and more dense (due to chemical differences) than the surrounding sea water, it might collect in pools such as those found in the Red Sea.

(b) The deep hydrothermal system. The circulation pattern could be controlled by one or more of the following physical properties of the system: (1) variation in the strength of heat sources near the base of the crust, (2) bottom topography, (3) discrete zones of high permeability, or (4) cellular convection. Only limited conclusions may be inferred about the heat-flow data. Hot intrusives rising to near the base of the oceanic crust, spaced at about 6 kilometers along our track could force the entire system. The pattern of steep scarps suggests that the surface might have undergone north-south extension and block faulting which could be a by-product of deep intrusive east-west trending dikes associated with sea-floor spreading. The occurrence of heat-flow maxima near topographic highs and

heat-flow minima near topographic lows may imply topographic control as proposed by Lister (1972). This correlation between topography and the heat-flow pattern, although approximate, appears to be more than a coincidence. The data seems to indicate that the convection is not entirely controlled by the major vertical faults. The heat-flow maxima and minima on the Galapagos Spreading Center, are not always located near the steep scarps (faults?)(Fig. 8). This is in contrast to the pipe model of Bodvarsson and Lowell (1972) and to observations in Iceland (Bodvarsson, 1961) and most continental geothermal areas (McNitt, 1965) where the hydrothermal activity at the surface is in close proximity to dike contacts and vertical faults (zones of high vertical permeability). This could imply that the young oceanic crustal rocks on this spreading center, and perhaps elsewhere, have a finer scale of permeability than rocks in continental geothermal areas.

CHAPTER III

CELLULAR CONVECTION IN THE OCEANIC CRUST

A. Theory and Discussion

The regularity of the modulation observed in the conductive heat-flow measurements at the Galapagos Spreading Center led me to look at cellular convection as a possible explanation. Cellular convection through permeable rock was first suggested by Elder (1965) as being the mechanism by which large amounts of heat might be removed from active spreading ridges or any oceanic thermal area. Elder described the general fluid dynamical problem. The following paragraphs will summarize and add to his description.

A. 1. Description of the fluid dynamical problem

Consider a horizontal slab of homogeneous saturated porous material of thickness H, horizontal extent L, permeability k and thermal conductivity K_m, saturated with a fluid of density ρ, specific heat c and kinematic viscosity ν. The temperature difference between the upper and lower surface is held at ΔT.

The fluid motion arises from buoyancy forces produced by imbalanced density variations in a field of non-uniform temperature. The fluid density is given by $\rho = \rho_0(1 - \alpha T)$ where α is the coefficient of thermal expansion.

Using Darcy's law (Darcy, 1856) I can modify the usual Navier-Stokes equation of fluid motion to obtain:

$$\frac{\partial \vec{q}}{\partial t} = -\nabla p - \frac{\nu}{k}\vec{q} + \vec{g} \qquad (1)$$

where $\vec{q}$ is the product of the porosity (a scaler) and the fluid velocity vector $\vec{v}$. $\frac{\partial \vec{q}}{\partial t}$ is small at low Rayleigh numbers and can be neglected except in special cases. Making the Boussinesq approximation (density variations are important only insofar as they generate buoyancy forces) the equation of motion becomes:

$$\rho_o \vec{q} = \frac{k}{\nu}\left[\nabla p - \alpha \vec{g} \rho_o (T - T_o)\right] \qquad (2)$$

Here $\vec{g}$ is gravitational acceleration and p is the departure of the pressure from its value when T is constant ($T = T_o$) everywhere.

Heat is transported by two mechanisms, convection at a rate $\rho c u \cdot \nabla T$ and conduction at a rate $K_m \nabla^2 T$. K_m must be approximated for the fluid-saturated medium.

The problem is now specified by five numbers k/v, H, L, $\alpha g \Delta T$, and K_m where the thermal diffusivity $K_m = k_m/\rho c$. Three dimensionless parameters now can define the system.

$\sigma = \nu/k_m$ = Prandtl number

$R = k \quad g \quad T \quad H/K\nu$ = Rayleigh number

$\alpha = L/H$ = aspect ratio

Another useful parameter is the power Q transmitted through the slab. $Q = \eta K_m \Delta T/H$ where η is the Nusselt number, a dimensionless conductivity. With no convection $\eta = 1$ if $\alpha \gg 1$. At values of the $R > R_c$, the critical Rayleigh number, convection begins and η increases with R. With horizontal, impermeable upper and lower boundaries $R_c \approx 40$. This has been shown theoretically (Lapwood, 1948) and experimentally (Elder, 1965). With the upper boundary open to free discharge and recharge R_c decreases to about 10 (Elder, 1967). If the upper boundary is not flat but has some relief (topography) any positive R is above R_c, but motion may be insignificant.

The simplest way to show that fluid motion must exist in a system with topography is to show the existence of non-zero vorticity (ζ) in the fluid. I now include the inertial term in the equation of fluid motion:

$$\text{vorticity} = \nabla \times \vec{q} \equiv \zeta$$

$$\nabla \times \left\{ \frac{\partial \vec{q}}{\partial t} = - \frac{\nabla p}{\rho_o} - \frac{\nu}{k} \vec{q} + \frac{\rho \vec{g}}{\rho_o} \right\} \qquad (3)$$

which reduces to

$$\frac{\partial \vec{\zeta}}{\partial t} = \frac{\nu}{k}\vec{\zeta} + \frac{\nabla\rho \times \vec{g}}{\rho_o} \qquad (4)$$

Horizontal density gradients are always present. This is most easily seen near the isothermal upper boundary where there must be liquid at different temperatures at the same vertical level. Therefore, with a non-zero thermal expansion coefficient, the last term in equation 4 must be non-zero implying the vorticity is also non-zero and fluid motion exists.

The relative importance of topography in controlling motion can be estimated by comparing the magnitude of the horizontal density gradients resulting from normal cellular convection and those caused by topography. The horizontal density gradient is proportional to the horizontal temperature gradient. In a normally convecting system this is about .5 Δ T/H. With topography of amplitude Δ Z and wavelength 2H, the horizontal temperature gradient is roughly $\frac{\Delta Z \, \Delta T}{H^2}$. Clearly, if ΔZ/H is of the order as .5 ΔT/H, topography can be important. On the Galapagos Spreading Center Δ Z's are one hundred to two hundred meters and H may be 3 km yielding a Δ Z/H, that, although less than .5 Δ T/H, is significant. It can also be seen from the analysis that the horizontal wavelength of the topography can

act to enhance or dampen the normal cellular convection pattern. On the Galapagos Spreading Center, the horizontal wavelength of the topography is roughly 6 km or the same as the implied hydrothermal convection system (Klitgord and Mudie, in press). This not only suggests that the topography might enhance cellular convection but also suggests that there may be a more profound reason for this similarity.

If the amplitude of the topography is greater, the system will become more affected by it until, in the end, topography completely dominates the circulation. As this limit is approached circulation continues but cannot be described as cellular. This could be the case on the Mid-Atlantic Ridge at 36°N (next chapter). The amplitude of the topographic undulations is as great as 2 km, an order of magnitude greater than the Galapagos Spreading Center. The point at which the departure from cellular convection occurs, and how dramatic this change is, depends on the nature of each system and its many complicated parameters.

The problem can be studied by utilizing computer-generated numerical solutions or laboratory models. Computer solutions are all complicated, expensive, and lack the confidence that can be gained from laboratory modeling.

B. Laboratory modeling

B. 1. Discussion

Three-dimensional models can be constructed to closely reproduce Φ, R and α in a scaled-down version of an actual hydrothermal system. The motion in such systems is inherently difficult to observe but has been shown by many investigators to be dominated by two-dimensional cellular rolls. Furthermore, the actual field situation is not well understood and thus can only be usefully modeled in a very over-simplified way.

Erickson and Simmons (1969) and Lister (1972) discuss the magnitudes of the various parameters that make up the Rayleigh number and stress that the principal unknown in an actual hydrothermal system is the permeability. It is clear that the Rayleigh number decreases away from a spreading ridge axis because of the inevitable decrease in the temperature differences (ΔT) and the average permeability. Local periodic changes in the strength of the heat source will also affect ΔT and hence the Rayleigh number. Hele-Shaw (1898) showed that cellular convective motion in simple porous medium is similar to that in a vertical cavity of width a $\ll$ H,L where the permeability $k \approx a^2/12$. The theory can be found in Lamb (1932, sec. 330). This model has the great advantage that the flow can be visualized and photographed.

B. 2. Model I

Utilizing a Hele-Shaw cell, I have attempted to model the Galapagos Spreading Center problem. The physical apparatus is described in Appendix 1. My first step was to construct a simple model (closed, horizontal boundaries with $\mathscr{A} \gg 1$) and conduct a series of experiments. With this I was able to reproduce results similar to those found by previous investigators: regular, equidimensional Rayleigh cells (Fig. 12). A Rayleigh cell is defined here as a cell bounded horizontally by a rising limb on one side and a descending cell on the other, i.e. its width is one-half the horizontal cellular wavelength. (λ) For Rayleigh numbers less than 500 (the upper limit of my experiments) the width of the Rayleigh cells was always between .8 and .9 times H. This situation corresponds to the theory of Lapwood (1948) and Donaldson (1962). Even with a large aspect ratio ($\mathscr{A} \gg 1$) end-effects were quite evident. In these models L is the length of the heated portion of the lower boundary and only the central 80% of the lower boundary was heated. A simple study of end-effects is contained in Elder (1967). Some additional observations are relevant to all my models: (1) I found the cells tended to become somewhat narrower as the Rayleigh number increased, up to several times R_c, where $R_c \approx 40$. (2) Most vertical motion was in narrow limbs (rising or descending).

Figure 12. Photograph of motion in a Hele-Shaw cell. There is no topography in this cell, i.e., the upper boundary is flat and closed. In this experiment the Rayleight number was 360. From left or right the vertical dark columns are alternately rising (darkest and widest at bottom) and descending limbs.

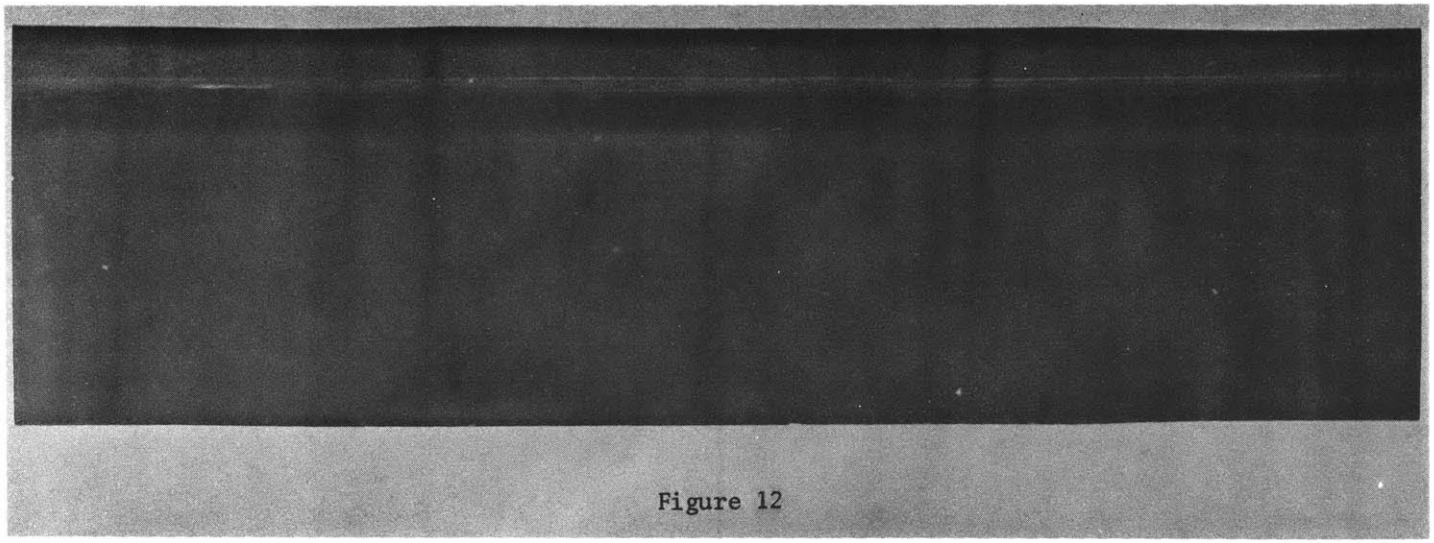

Figure 12

(3) For any given Hele-Shaw cell with $\alpha^2 >> 1$, the system tends to approach a constant value of λ corresponding to its value at $L \to \infty$ (i.e. no ends). But the system prefers an even number of Rayleigh cells implying that unless L/λ is an integer, L may have a substantial influence. To further complicate the matter, the ratio of L to the total length of the apparatus has a second order effect. The result is that unless a set of complementary parameters is found this simple model displays a long period instability. If it has too few pairs of Rayleigh cells it will slowly create another pair. But it will then have too many pairs of Rayleigh cells and will slowly destroy a pair.

Finally my experiment showed a hysteresis in behavior similar to that observed by Elder (1967). That is, I produced different Rayleigh cell arrangements at any given R depending on whether I had increased R to that value or decreased R from some higher value. This is an interesting phenomena but seemed to disappear when I went on to models with topography on the upper boundary.

B. 3. Model II

The next step was to test the effect of impermeable topography (at the upper boundary) on the cell's motion. The

topography was modeled by brass flat stock (of width $\approx$ a) soldered to the boundary's copper pipe, cut to match the Galapagos and inserted in the cell's cavity. In my first experiment H was scaled with the topography to model a 5 km deep circulating system and tests were run over a series of Rayleigh numbers from R = 10 to 700. Figure 13 illustrates the effect of topography on the positions of the cells. As suggested by Lister (1972), descending limbs tend to seek out and hold onto topographic lows. The same relation exists between ascending limbs and topography highs. These photographs also show that in the interior regions of the system the cell positions are less constrained by the topography. The system displayed a long period instability. The horizontal wavelength (λ) of the motion does not seem to be affected by the topography. As a result, the 5 km deep model yielded a wavelength of 8-9 km and did not match the wavelength (6 km) observed at the Galapagos Spreading Center.

Using the observed cell width to height ratio of 0.8 to 0.9, the indicated circulation depth is 3 to 4 km. In the next experiment I reduced the modeled system depth to 3.75 km. The results were generally similar to those found with the 5 km experiment except that the system displayed excellent stability and a closer match to the observed data was obtained (Fig. 14).

Figure 13. Photographs illustrating the effects of topography on the motion in Hele-Shaw cell. The topography, simulating the Galapagos Spreading Center, can be seen near the upper edge of the pictures and is scaled to a 3.75 km deep circulation system. The horizontal line just below this is part of the laboratory apparatus. The dark, nearly vertical lines are the rising and descending limbs of Rayleigh cells. The three photographs show (a) a rising limb in the center, flanked by two descending limbs, (b) a descending limb in a topographic low, (c) a rising limb under a topographic high. It can be seen that below the upper boundary the cells are not as rigidly constrained by the topography.

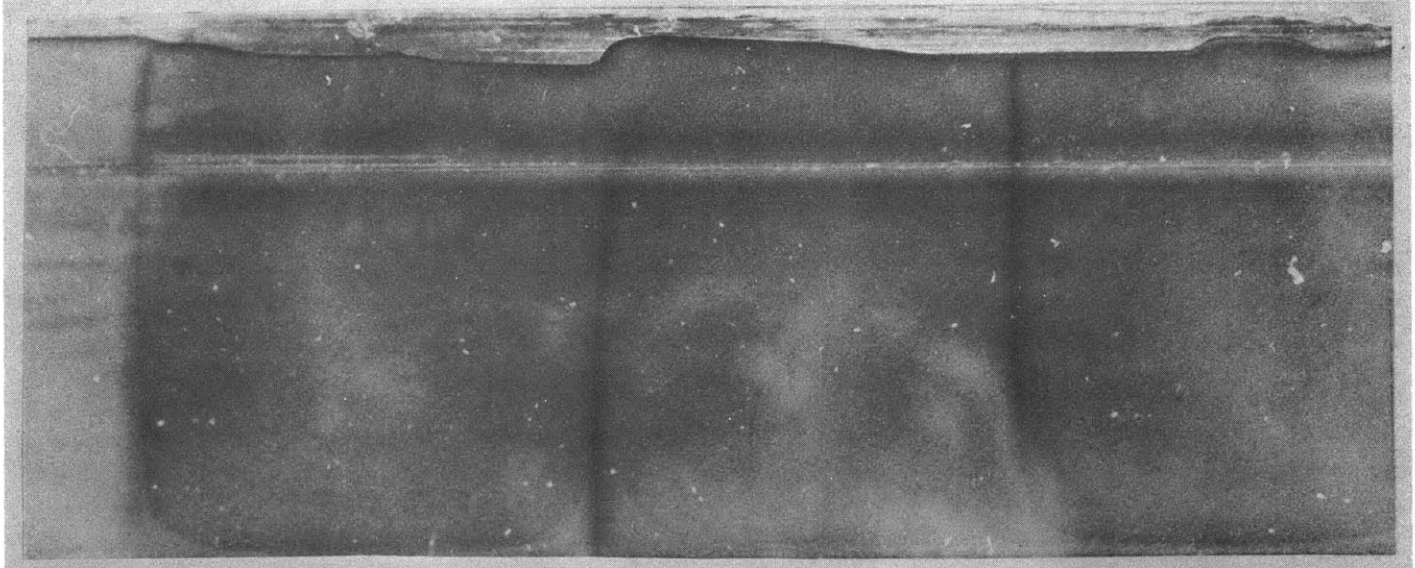

a

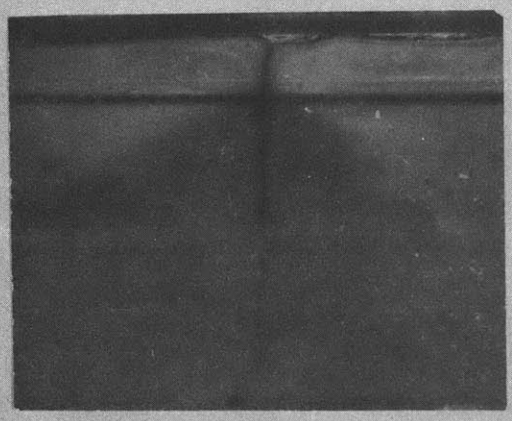

b

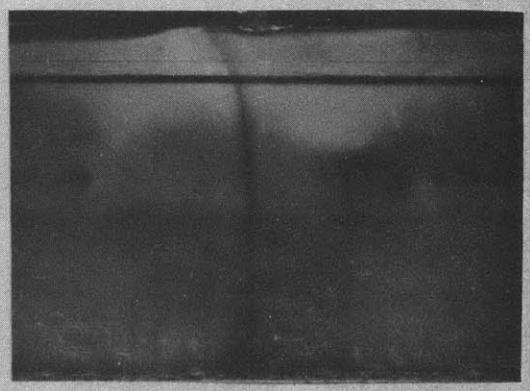

c

Figure 13

Figure 14. Comparison of observed heat flow (HFU) on the Galapagos Spreading Center and fluid motion in a Hele-Shaw cell modeling the Galapagos Spreading Center topography. The dark vertical columns mark the rising and descending limbs. Rising limbs appear to touch the lower boundary. Descending limbs touch the upper boundary. The heat flow curves are taken from the average presented in Figure 6. The system parameters modeled by the Hele-Shaw cell are (a) R=330, η = 7.0, H=3.75 km, (b) R=270, η =8.2, H=2.9 km.

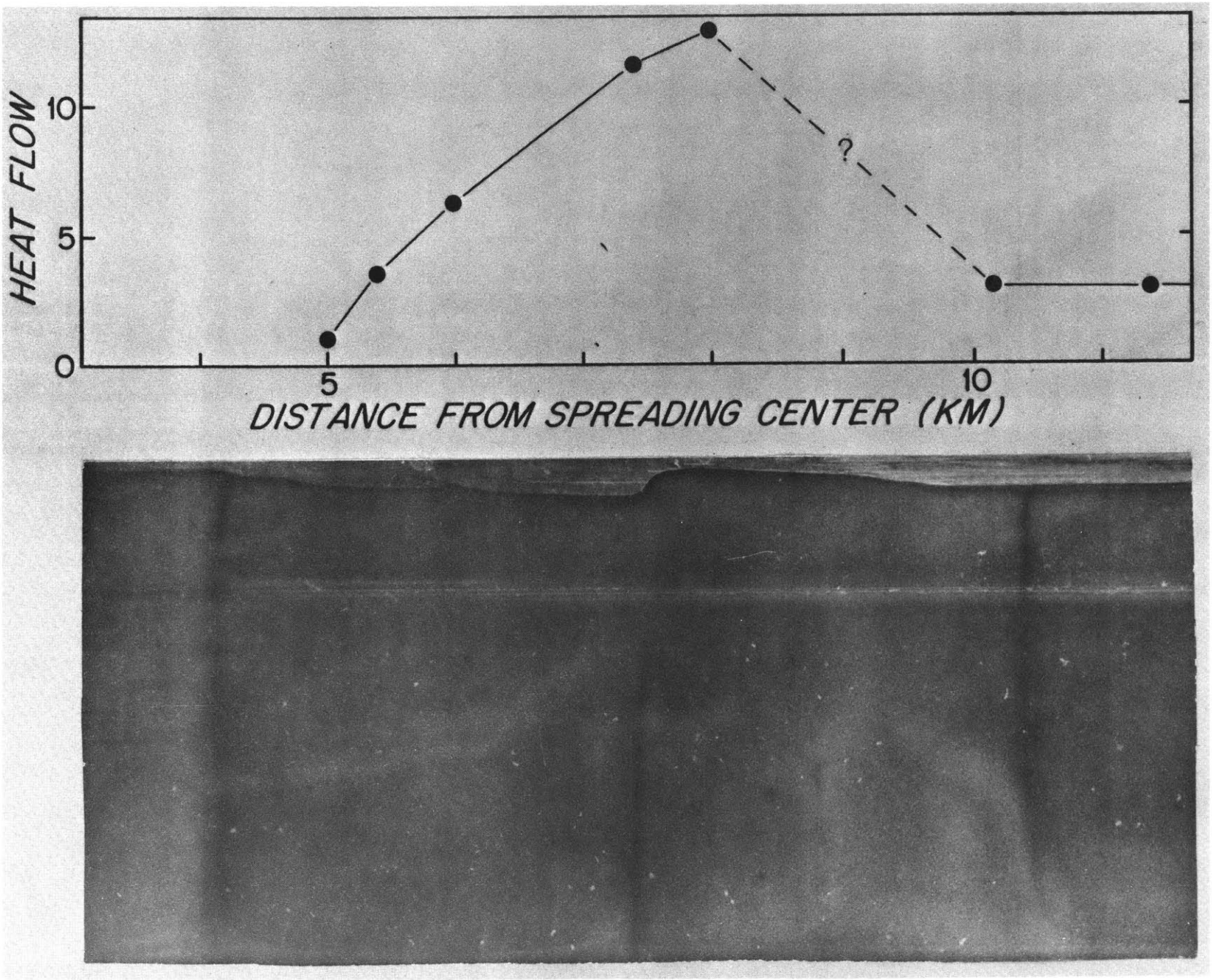

Figure 14a

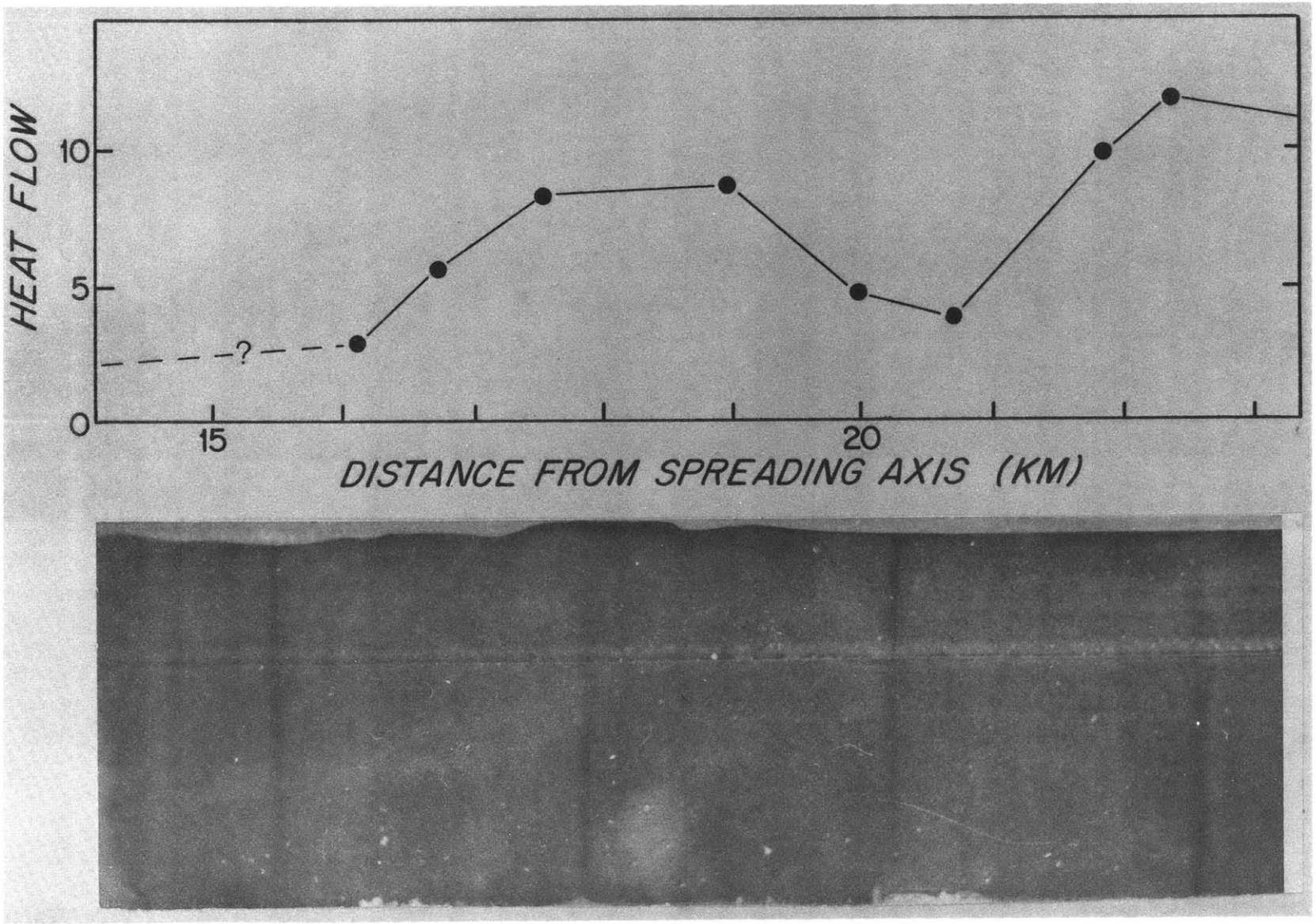

Figure 14b

I then tried a model depth of 2.9 km. This experiment was almost completely stable from R = 100 to 360 (the highest R modeled). Between R = 100 and 0 the motion is apparently too slow and diffuse for the suspended aluminum particle photographic technique. Significant motion was observed down to R = 17. The topography enhanced the motion up to R = 360. This can be seen in Figure 15. The Nusselt number is higher and hence the heat transfer is more efficient than in the models without topography. This same effect was also evident within individual experiments. Portions of the Hele-Shaw cell with subdued or no topography always had a higher Rayleigh number and hence a lower Nusselt number. The convection pattern displays instabilities when, for example, the wavelength (λ) does not match to topography or when there is no topography or when the end-effects become prominant. This causes variations in the heat transfer efficiency (Fig. 15).

At higher Rayleigh numbers $500<R<1200$ a substantial decrease in the wavelength (λ) occurs. Such high Rayleigh numbers may occasionally be important locally on very young (less than 0.1 m.y. old) crust, but I did not study them in detail. At R = 1200 I found $\lambda = 0.9H$ and on experiments where R was between 500 and 1200, λ was always less than 1.6H.

Figure 15. Heat transfer characteristics for convection in porous medium with the Galapagos Spreading Center topography modeled on the upper boundary; Nusselt number (η) as a function of Rayleigh number (R). Symbols indicate data from four different system depths (H). For $50 < R < 300$, data fits the line $\eta = .021R$. For $R < 50$, convection gradually decreases to a negligible level. For $R > 300$, values of η are scattered, but these are all data points from an $H \approx 5$ km model and this model displayed a long term instability. The line $\eta = .025R$ is from Elder (1965) for a cell without topography.

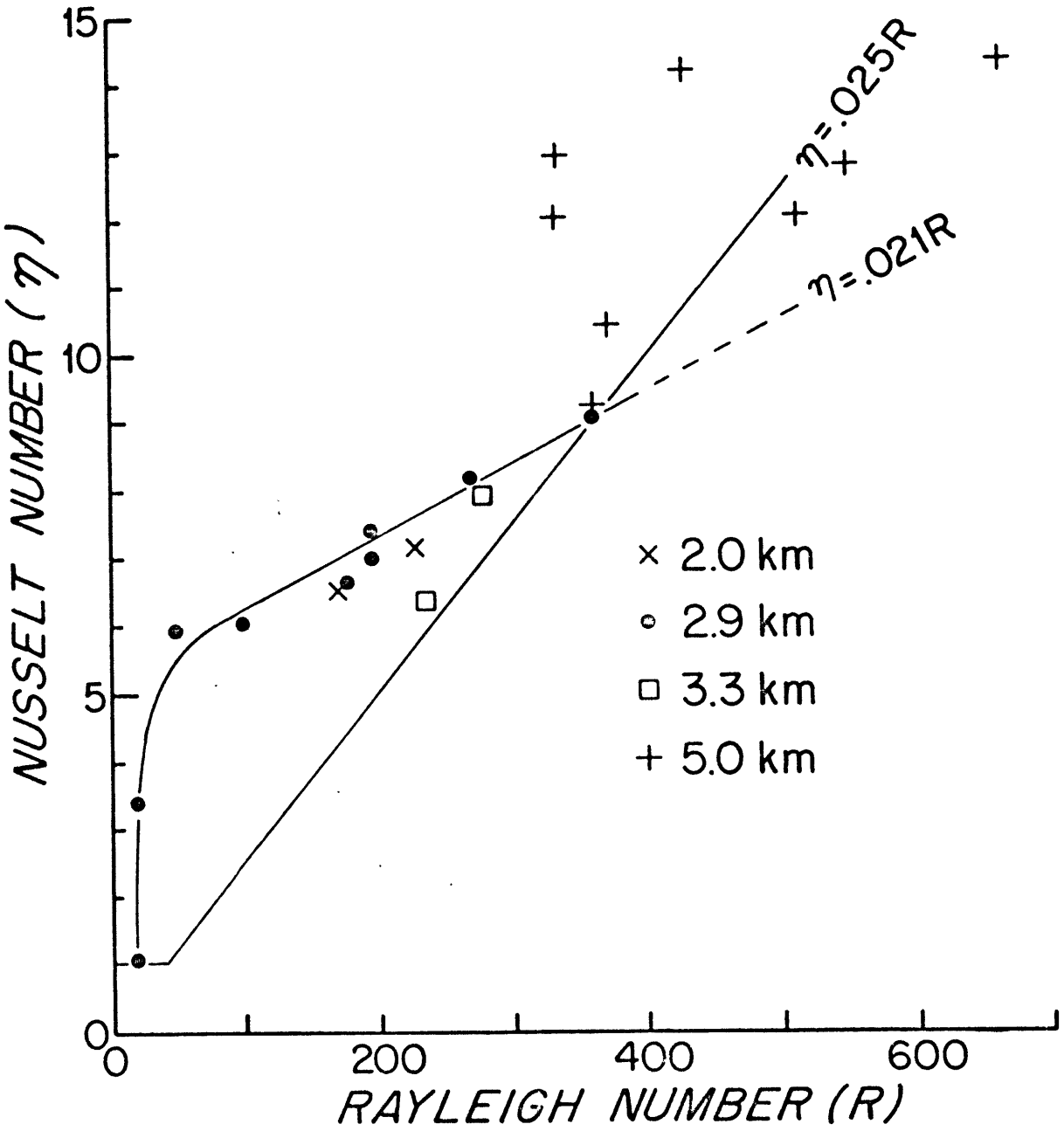
15
10
5
0
0
200
400
600
NUSSELT NUMBER (η)
RAYLEIGH NUMBER (R)
η=.025R
η=.021R
× 2.0 km
∘ 2.9 km
□ 3.3 km
+ 5.0 km

C. Discussion

These observations are based on experiments with a Hele-Shaw cell modeling a completely closed and isothermal upper boundary. This type of hydrothermal system increases subsurface heat transfer efficiency and redistributes heat but all the heat still must be conducted through the upper boundary. Numerical studies and experiments with a Hele-Shaw cell having an upper boundary completely open for free discharge and recharge have yielded results similar to the closed cell (Elder, 1967). I conducted a few preliminary experiments in which a Hele-Shaw cell opened at its lid into a wide fluid filled cavity. On this upper boundary I modeled an arbitrary topography in which $\Delta z/H \approx .2$. I was unable to keep the fluid in the wide cavity well mixed and terminated the experiment. Nevertheless, I found the cell positions stable, controlled as before by the topography with cell dimensions relatively unaffected. These were only preliminary observations and a more complete, well controlled study is needed.

In an actual hydrothermal system, it is reasonable to expect that the permeability (k) slowly decreases with increasing depth. The effect of this phenomenon has not been studied but it can be modeled with a Hele-Shaw cell. However, because this simply makes R a function of depth and in my experiments I saw

very little change in topographic control on cell dimensions with $100<R<600$ I have no reason to assume that these variations in k should drastically alter the cellular convection pattern.

Variations in the strength of the heat source or the bottom boundary temperature of a hydrothermal system certainly exist and could be modeled. Unfortunately nothing is known of them. The same is true of relief along the bottom boundary. These factors could have a strong influence on the positions of the cells, but as with upper boundary conditions only in extreme cases would I expect the cellular nature of the system destroyed or the cell wavelength drastically affected. The same thing is true of variations in permeability along the upper boundary. Elder (1965) studied this in systems with $\alpha = 1$, but this is not very applicable. Also very little is known about the permeability, or more important, the penetrability of the sediments along this boundary.

Studies of continental geothermal areas especially those <u>not</u> covered by thick sedimentary sequences (e.g. Iceland and Yellowstone Park) have yielded valuable information about the source and distribution of permeability in igneous rocks. This subject is discussed by Bodvarrson (1961). To summarize he feels the main sources of permeability in basalts are (1) tubes and openings at the contact of lava beds, (2) columnar structure in

and fissures along the walls of intrusive bodies,and (3) recent faults.

Finally, the motion in a Hele-Shaw cell is only two-dimensional. This is sufficient whenever the motion in the actual system is dominated by two-dimensional rolls. If the motion has a significant three-dimensional component the surface heat-flow pattern would change accordingly. But the cellular wavelength and the topographic influence on cell positions seem to be such strong physical properties my experience makes me believe they would not be substantially affected by the addition of a third dimension.

D. Conclusions

1. The horizontal wavelength of hydrothermal convection is a strong function of the depth of circulation ($\lambda \approx 1.7H \pm 10\%$ for $R < 500$) and a lesser function such parameters as the Rayleigh number, topography or heat source distribution.

2. The position of the cells is a function of the topography and/or the heat source distribution.

3. The vertical fluid motion is concentrated in narrow limbs.

4. Vertical relief in either the upper or lower boundary or variation in heat source strength can enhance the motion and therefore the heat transfer, at low Rayleigh numbers.

5. The Hele-Shaw cell technique is a powerful tool and can and should be used to help understand many of the problems associated with hydrothermal circulation in the oceanic crust. The whole subject of free discharge and recharge needs more study as do the affects of vertical,and horizontal variations in permeability and horizontal variation on the bottom boundary condition.

6. More field data is especially needed to determine to what extent actual hydrothermal systems are three-dimensional and what the distribution of sediment and rock permeability is.

7. Because of the complexity of the problem this type of simple laboratory study cannot be conclusive in determining the controlling parameters of sea-floor spreading hydrothermal circulation. However, it does provide valuable insight. Much more laboratory and field work is obviously necessary before it will be possible to accurately describe actual spreading ridge hydrothermal systems.

CHAPTER IV

HEAT LOSS FROM THE EARTH

A. Introduction

The heat loss from the Earth, in regions where conductive heat flow is > 99% of the total (i.e., the continents, continental margins, and old ocean basins), can be estimated fairly accurately utilizing conductive heat-flow measurements. On the Galapagos Spreading Center and probably most active oceanic ridges hydrothermal circulation is important. Unfortunately no techniques exist which will permit the direct measurement of this component of the Earth's heat loss. As a result we must use more indirect, theoretical methods to estimate the total heat loss through young oceanic crust.

B. Continental

Consider the total heat loss of the Earth as separable into three components: continental, oceanic background (steady-state), and oceanic due to lithospheric formation (transient). Including the continental shelves and slope, the continental component is derived from an area of 1.48×10^{18} cm^2 and an average heat flux of 1.46×10^{-6} HFU (Lee, 1970), resulting in a heat loss of

2.16×10^{12} cal/sec ±10%. The heat loss from volcanoes, hot springs, and geysers, although sometimes spectacularly evident on a local scale, is estimated to be only 5×10^{10} cal/sec (Elder, 1965) and is insignificant when compared with the total (Q_e).

C. Oceanic Background

The second component, the oceanic background, is the heat flux through the surface of the ocean floor after the spreading lithospheric plates have cooled. Here we estimate it by examining heat-flow values from the oldest identified parts of the sea floor. Mesozoic-age magnetic anomalies have been postulated in the NW Atlantic and W Pacific (Larson and Pitman, 1972). The average heat flux for these regions is 1.12 ±.04 (standard error) HFU for the Atlantic, and 1.17 ±.03 HFU for the Pacific. The Wharton Basin of the Indian Ocean, which from deep sea drilling appears to have an age greater than 90 million years (von der Borch, Sclater, et al., 1972; Veevers and Heirtzler, 1973), has an average heat flow of 1.21 ±.06 HFU (McKenzie and Sclater, 1969). From these data we obtain an overall average for this background component of 1.15 ±.05 HFU. However, the theoretical cooling time of a 100 km thick lithosphere plate would require us to correct this background to a value of

1.10 ±.05 HFU, whereas for a 75 km lithosphere this correction is less than 1 percent; here we adopt a corrected value of 1.12 ±.06 HFU. The area of the oceans (Menard and Smith, 1966), including marginal seas and continental rises, is 3.62×10^{18} cm^2 resulting in a total rate of heat loss from the background component of 4.06×10^{12} cal/sec ±10%. Most of this heat originates below the lithosphere. Again, the higher average heat flux from volcanoes (exclusive of actively spreading ocean ridges) and marginal seas has not been considered, as the effect on the total (Q_e) is insignificant ($< 1\%$).

D. Sea-floor Spreading

The final component is the heat (Q_ℓ) continually being released as a result of sea-floor spreading. Since this quantity is estimated from a theoretical expression, its accuracy is largely dependent on the physical model and associated parameters assumed for lithospheric formation. The seismic, topographic and thermal data reviewed in Williams and Poehls (in preparation) indicate that most oceanic lithosphere attains near thermal equilibrium conditions prior to subduction. After 50 m.y. a lithosphere has lost more than 95% of its transient heat and over 99% after 100 m.y. Although some subduction zones (e.g., Peru and Middle America trenches) are subducting relatively

young lithosphere at a relatively rapid rate, the effect on the calculation of total (Q_e) heat flux is small (< 1%).

We have utilized a simplified expression $Q_\ell = P\ell dvT_A f$, in which the principal uncertainties are the equilibrated lithospheric thickness (ℓ) and basal temperature (T_A). In this expression we ignore effects such as adiabatic compression, thermal expansion, and heat sources within the lithosphere that would reduce Q_ℓ, as well as effects of latent heat of crystallization and hydration/dehydration of crustal rocks that would increase Q_ℓ. These are not insignificant effects but their overall influence on Q_ℓ is much smaller than uncertainties in ℓ and T_A; thus we omit further discussion of them here.

We have assumed values for the basal temperature (T_A) ranging from 1000°C to 1400°C (Forsyth and Press, 1971; Verhoogen, 1973). The lower value is based on the temperature required to melt the rock and the upper temperature is constrained by seismic velocities. The range of values chosen for equilibrated lithospheric thickness (ℓ) is 76 to 100 km and derives primarily from seismic data (Forsyth and Press, 1971). We have measured the total length (d) of all oceanic spreading centers as 53,700 km ±5%, and have estimated the average half spreading rate (v) as 2.74 cm/yr ±5%. The specific volumetric heat capacity (P), taken as 0.90 ±.05 cal/cm^3°C, is deduced from Schatz and Simmons'

(1972) measurements of lattice thermal conductivity (K_L) and diffusivity (κ_L) where $P = K_L/\kappa_L$. Their results indicate that this value varies little for the minerals and temperatures encountered in the lithosphere.

The factor f accounts for effects that lithospheric creation has on the oceanic background component of heat loss. If the heat flux into the bottom of the lithosphere is constant, f = 1.0. This model would hold if sub-lithospheric heat derives primarily from internal heat sources (e.g. radiogenic heat) and if all this heat is efficiently transported to the base of the lithosphere. In contrast, if the presence of a high temperature young lithosphere suppresses some of the asthenospheric heat flux, for example McKenzie's model (McKenzie and Sclater, 1969), f approaches 2/3 (Sleep, 1969). We have taken $f = .84 \pm .16$ as a compromise between these models, where the estimated error covers the range of uncertainty of the extreme models.

E. Discussion

Table III shows the calculations for three different sets of parameters. We assume the median value between the two extremes represented by solutions 1 and 3; the total of the three components of the Earth's heat loss is then 10.2×10^{12}

TABLE III. SUMMARY OF SEA-FLOOR SPREADING HEAT LOSS CALCULATIONS

Solution No.	ℓ (km)	T_A (°C)	K	Q
1	76	1050	7.5	2.9
2	85	1300	6.8	3.9
3	100	1400	7.5	5.0

K is in 10^{-3} cal/cm-sec°C

Q is in 10^{12} cal/sec

cal/sec which represents a 32% increase over Lee and Uyeda's (1965) estimate. This results in a mean heat loss per unit area of over 2.2 HFU for the oceans and about 2.0 HFU for the Earth. Lithospheric cooling represents about 40% of this total. More than 50% of the lithospheric cooling occurs before the sea floor is two million years old. Measurements of conductive heat flow on young crust (Galapagos Spreading Center, Chp. 2) indicate that only a small portion of this heat is released by thermal conduction through rocks and sediment at the sea floor. Sea water quenching of extrusive lavas (seismic layer 2) likewise can only account for a small portion of the heat loss. If hydrothermal circulation in the oceanic crust out to 2 m.y. is primarily responsible for removing the remaining heat, this process accounts for approximately 20% of the total heat loss of the Earth. There is some evidence for hydrothermal circulation in much older crust (Williams and Poehls, in preparation) which would make this a minimum estimate.

It is interesting that, because most of the heat is released through the components of lithospheric formation and oceanic background, the heat flow through the Earth's surface is significantly biased toward the southern (ocean hemisphere). Due to the probable complexity of the kinematics and dynamics of

material in the Earth's interior (McKenzie, 1968) this does not necessarily indicate long-term asymmetry in the cooling of the Earth. However, models of the Earth no longer are constrained by the previously accepted equality of oceanic and continental heat flux.

For comparison we estimate the total rate at which man uses energy (coal, oil, and natural gas) is approximately 2×10^{12} cal/sec. The energy dissipated by tides in the Earth, water, and atmosphere is approximately 0.7×10^{12} cal/sec (Hendershott, 1973). Because only a small portion of tidal dissipation occurs in the solid earth, it contributes a negligible part of the total heat loss. Finally, the heat intercepted by the Earth from solar radiation is about 4×10^{16} cal/sec, about 4000 times the rate of heat loss from the Earth's interior. From first order error analyses, we estimate the accuracy of this new value for the Earth's rate of heat loss, 10.2×10^{12} cal/sec, at ±15%. The principal uncertainty derives from the unknown parameters of the oceanic lithosphere (Table 1). A substantial fraction (40%) of the heat loss derives from the transient cooling of new oceanic lithosphere, and it seems probable that this mechanism is the "safety valve" for excessive heat generated in the Earth's interior.

CHAPTER V

GEOTHERMAL STUDY OF THE MID-ATLANTIC RIDGE AT 36°N

A. Background

Although hydrothermal circulation is assumed to be important on all active spreading centers, the Galapagos Spreading Center is just one example and possibly not typical. Spreading rates on the Earth's sea-floor spreading system vary over an order of magnitude and topography and faulting patterns show considerable differences. The conducted heat flow on the Galapagos Spreading Center is higher than other ridges presumably because high sedimentation rates seal off the surface discharge. This implies that on most ridges an even higher percentage of the total heat loss is convected away. Fault patterns and topography may prevent cellular convection from developing, requiring some less efficient form of convection to remove the heat. Without some basis for comparison one can only speculate about these questions.

For this reason, I decided to investigate another spreading center. A section of the Mid-Atlantic Ridge crest between 36° and 37°N latitude (Fig. 16) is currently the subject of an intensive geophysical and geological investigation. The project,

Figure 16. Mid-Atlantic Ridge near 36°N. Bathymetric contours are in uncorrected fathoms. Hatched region marks FAMOUS study area.

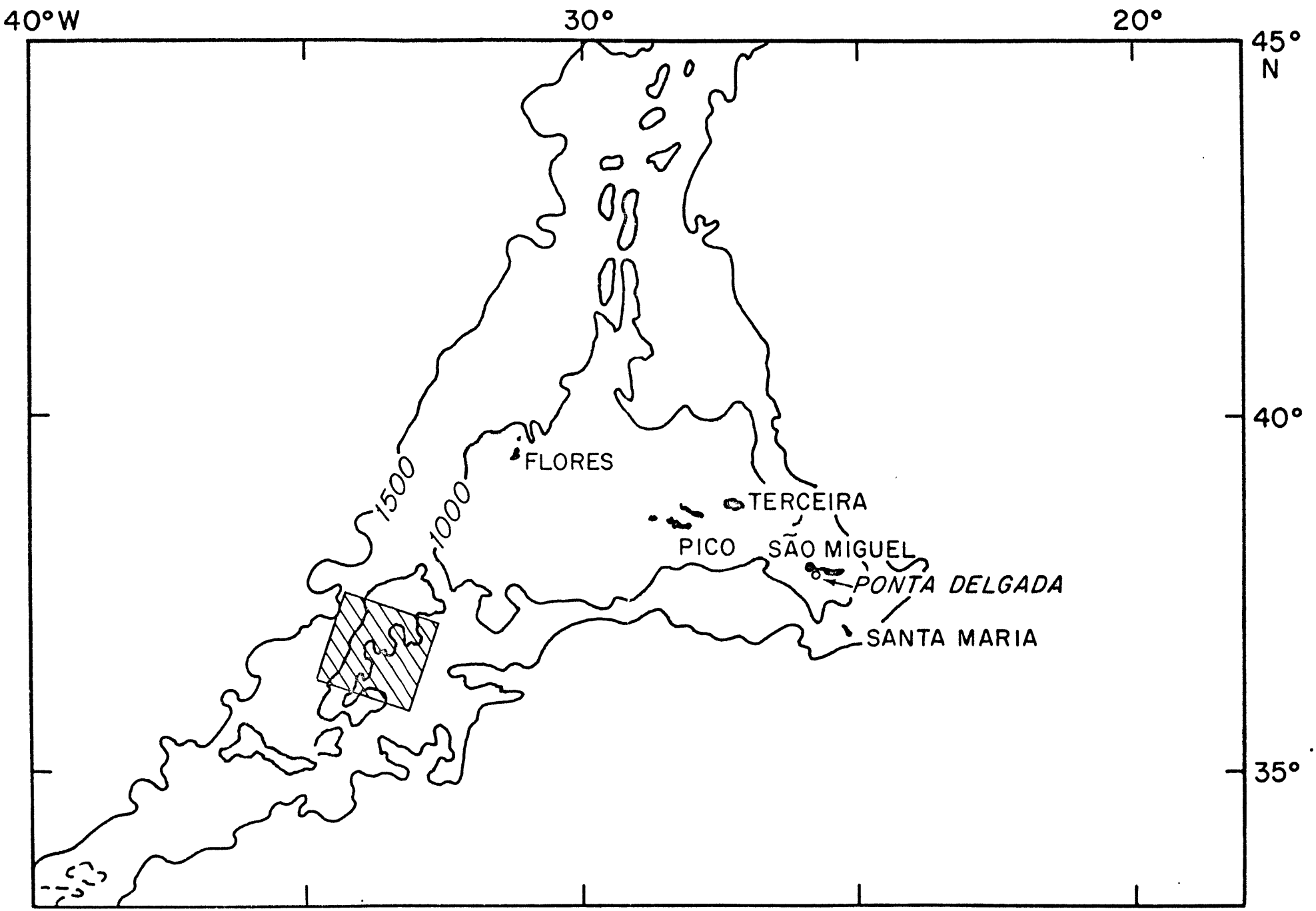
40°W
30°
20°
45°
N
40°
35°
1500
1000
FLORES
TERCEIRA
PICO
SÃO MIGUEL
PONTA DELGADA
SANTA MARIA

known as the French-American Mid-Ocean Undersea Study (FAMOUS), is described by Heirtzler and Le Pichon (in press). To summarize, the area is about 400 km southwest of the Azores and is situated on the lower portion of the Azores platform. The sea floor is spreading at a half rate of about 1.15 cm/yr. The spreading center is marked by a well developed rift valley/rift mountain sequence and is offset by small (20 km long) transform faults about 40 km apart. In general, the region can be described as extremely rugged and sparsely sedimented. This is far from ideal, but because required ship-time, personnel and equipment were available I decided to attempt a detailed survey.

Heat-flow surveys were attempted in four different areas on Cruise 77 of R/V ATLANTIS II (August 1973); two were along terraces on the rift valley walls, one on the western rift mountain and one at the junction of a fracture zone and rift valley (Fig. 17). Only the latter two can be considered successful and I describe these results in the following sections.

B. Fracture Zone "B"

B. 1. Description of the area

The study area is located at the western intersection of a small E-W trending fracture zone (FZ"B") and a short

segment of the Mid-Atlantic Ridge (Fig. 17). This intersection is typical of others in this region; it is marked by a pronounced topographic depression. Its central floor is a roughly 60 km^2 area of relatively subdued topography with a mean depth of about 2800 m. It is ringed by rift mountains rising over 2000 m above the floor. These mountains are cut in the south by the rift valley which rises 200 m above the floor. On the east there is a transform fault extension rising up 800 m and, on the northwest side of the floor, the fracture zone is marked by a narrow valley whose mean depth is about 2400 m.

The central floor appears to have a very thin sediment cover. However, the southern extension of the rift is unsedimented. The thickness of the sediment probably never exceeds a few meters. No sediment is seen on seismic air gun records (minimum resolution is not much better than 100 m). Nor is sediment seen on 3.5 kHz and 4.0 kHz seismic profiler records, either ship mounted or deeply towed. These latter records, however, do show a return characteristic of thin (2-4 m) sediments. Bottom photographs of the floor show sediments broken frequently by rocky ridges. Finally, failure to penetrate the bottom on 12 of the heat-flow stations and partial penetration on several others tends to verify the other evidence for thin sediment cover.

Figure 17. Three-dimensional model illustrating the location of the heat flow surveys on the Mid-Atlantic Ridge at 36°N. Sites indicated by A and B are not discussed in the text. The western rift mountain survey area is outlined by the dashed line indicated by C and the fracture zone "B" survey area is D. Heavy dark lines mark fracture zone "B" and the axes of the adjacent rift valleys.

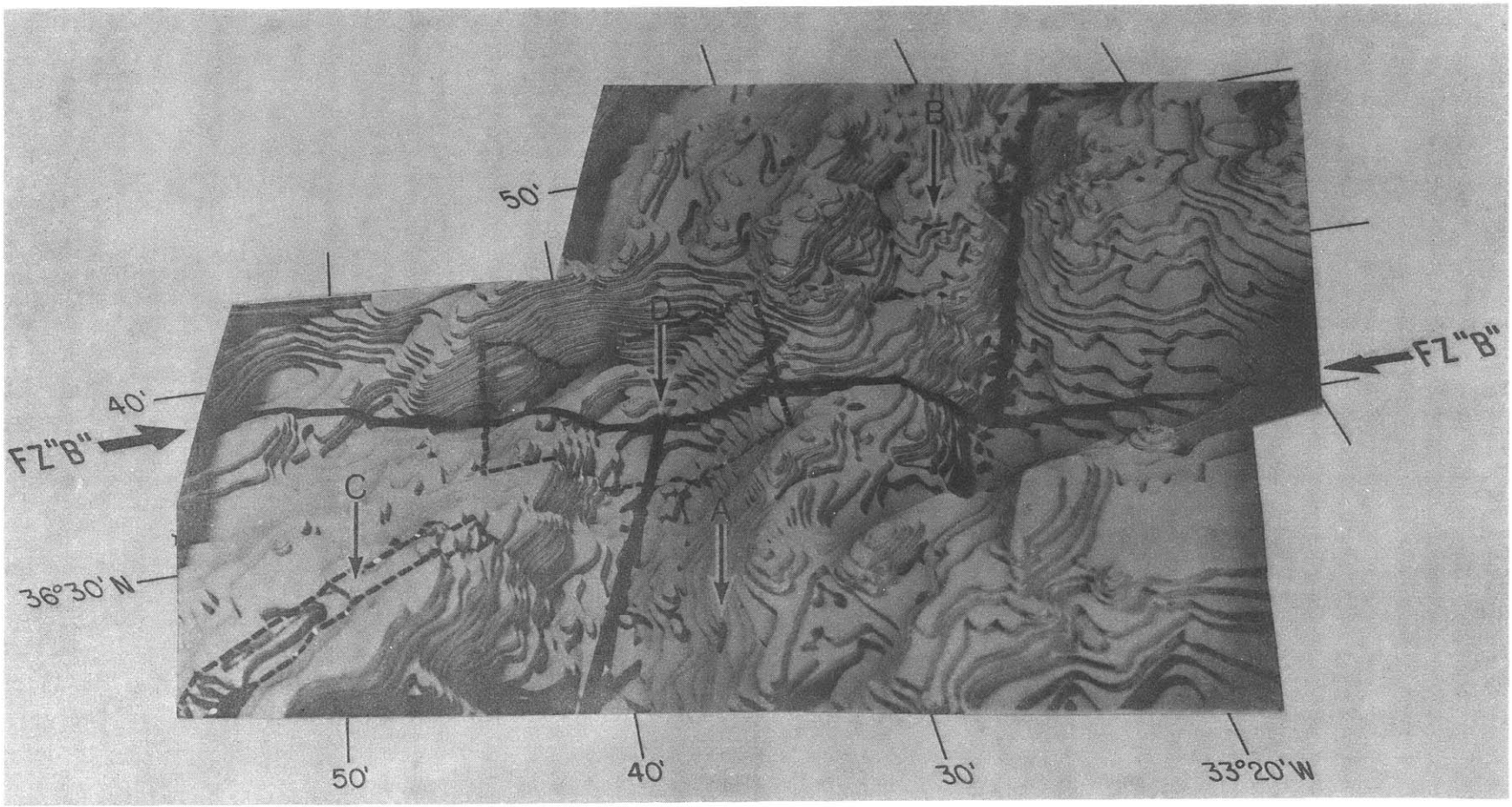

Figure 17

The transform fault appears seismically active as determined by a sonobuoy earthquake study conducted by Reid and MacDonald (1974). The gross features of the topography seem to indicate that the fault is a wide, diffuse region occupying about the same area as the spreading segments north and south of it. On closer inspection, the saddle lying between the study area and the eastern terminus of the transform fault is cut by a wide ($\sim$2 km), shallow ($\sim$ 120 m) trough. At the bottom of the trench is a narrow ($\sim$ 300 m), shallower ($\sim$30 m) notch which appears to mark the actual fault. However, this notch in places lies nearly 2 km south of Reid and MacDonald's earthquakes. The eastern five stations shown in Figure 9 lie at the bottom of the notch. Finally, an extensive suite of hydrothermally altered rocks has been dredged from several locations along the fault (Bryan, personal communication). None of the other geophysical or geological techniques employed have substantially helped define the location or nature of the fault or fault zone.

B. 2. Measurements and techniques

Forty-three of the new measurements (Fig. 18) reported in Table IV were obtained in fracture zone "B". All temperature gradients in the sea floor were measured with probes designed for multiple penetrations of the sediments. Two types of

TABLE IV

Station No.	Lat. N	Long. W	Water Depth	T	P	■	Q	Comments	NAV
16.1	36°40.0'	33°43.3'	1350	3.76	0.9	3	0.8		D
.3	36°40.5'	33°41.3'	1400	3.73	0.6	2	2.2	not equilibrated	D
.4	36°40.8'	33°40.6'	1400	3.76	0.8	3	3.8		D
.5	36°41.1'	33°40.3'	1370	3.76	0.4	2	3.3		D
17.1	36°41.9'	33°38.1'	1230	3.76	2.6	3	0.7		D
21.1	36°38.3'	33°39.1'	1350	3.80	1.5	2	0.7		S
.2	36°38.2'	33°38.9'	1400	3.80	0.9	2	0.8		A
.4	36°37.9'	33°38.3'	1400	3.83	0.6	2	0.9		A
.5	36°37.8'	33°38.1'	1400	3.85	0.4	2	1.8		A
.6	36°37.5'	33°37.5'	1425	—	0.5	1	1.8		S
22.1	36°35.8'	33°36.8'	1550	3.78	2.5	3	2.8		A
.2	36°35.9'	33°36.7'	1550	3.78	1.9	2	5.6		A
.3	36°36.1'	33°36.7'	1550	3.78	2.5	3	3.1	not equilibrated	A
.4	36°36.3'	33°36.7'	1550	3.79	2.5	3	1.1		A
25.2	36°26.4'	33°54.8'	650	—	0.4	2	1.7		R
.3	36°26.9'	33°54.1'	650	—	0.4	2	2.0		R
.6	36°27.1'	33°53.0'	650	—	0.4	2	7.6		R
35.3	36°45.0'	33°19.6'	1050	4.09	1.9	2	≥3.4		D
.4	36°45.8'	33°19.8'	1085	—	1.0	1	≥3.0		D
36.1	36°46.0'	33°19.9'	1010	4.12	2.2	3	≥3.5		D
.2	36°45.8'	33°19.5'	1040	4.25	1.0	1	≥2.4		D
.3	36°45.7'	33°19.7'	1050	4.72	2.1	3	≥4.1		D
41.1	36°35.5'	33°38.9'	1460	3.78	2.5	3	0.7		A
.2	36°35.5'	33°38.6'	1500	3.78	2.5	3	0.4		A
42.1	36°36.3'	33°38.0'	1500	3.79	2.5	3	2.6		A
.4	36°36.2'	33°38.8'	1550	3.79	1.7	2	≥3.4		A
43.1	36°36.3'	33°35.4'	1550	3.80	1.9	2	3.9		S
.2	36°36.3'	33°34.9'	1520	3.80	2.2	3	≥8.3		S
.3	36°36.4'	33°34.5'	1500	3.80	1.8	2	≥9.4		S
46.1	36°38.1'	33°34.8'	1525	3.77	0.7	2	3.6		S
.2	36°37.9'	33°34.2'	1475	3.78	0.7	2	3.6		S
.3	36°37.7'	33°33.8'	1450	3.79	0.8	2	3.2		A
.4	36°37.4'	33°33.5'	1425	3.78	0.8	2	6.9		A
.5	36°37.1'	33°33.3'	1425	3.77	0.8	2	6.3		A
.6	36°36.7'	33°33.3'	1425	3.77	0.6	2	5.6		A
.7	36°36.3'	33°33.2'	1425	3.78	0.7	2	7.9		A
.8	36°36.0'	33°33.0'	1425	3.78	0.9	2	15.4		A
47.1	36°36.7'	33°34.3'	1470	3.78	2.5	3	8.8		A
.2	36°36.5'	33°34.1'	1450	3.78	2.5	3	13.6		A
.3	36°35.7'	33°33.8'	1480	3.78	1.8	3	≥4.6		S
50.1	36°35.9'	33°34.6'	1550	3.78	2.5	3	6.5		A
.2	36°35.7'	33°34.6'	1550	3.78	1.7	2	≥5.3		A
.4	36°34.8'	33°34.7'	1525	3.78	1.0	1	≥2.5		A
51.1	36°37.0'	33°34.2'	1480	3.78	0.6	2	5.9		A
.2	36°36.9'	33°33.7'	1460	3.78	0.7	2	8.4		A
.3	36°36.9'	33°33.4'	1425	3.77	0.6	2	13.1		A
.4	36°36.9'	33°32.8'	1410	3.79	0.6	2	9.1		A
.5	36°36.8'	33°32.5'	1375	3.77	0.6	2	7.6		A
.6	36°36.8'	33°32.2'	1350	3.76	0.7	2	6.5		A
.7	36°36.8'	33°31.5'	1250	3.76	0.9	2	4.4		A
.8	36°36.8'	33°31.0'	1150	—	0.6	2	4.7		A
60.1	36°27.9'	33°46.6'	550	—	0.3	1	20.6		R
.4	36°27.3'	33°48.3'	600	—	0.4	1	≥11.1		R
61.2	36°29.4'	33°52.3'	720	—	0.7	2	3.4		R
65.1	36°24.6'	33°37.2'	1190	3.75	0.8	2	3.1		S
.2	36°24.8'	33°37.0'	1160	3.74	0.7	2	7.5		S
.3	36°25.1'	33°36.9'	1155	3.75	0.7	2	2.7		S
.4	36°25.3'	33°36.7'	1130	3.75	0.8	2	4.8		S
68.1	36°26.1'	33°56.5'	950	—	0.8	2	0.4		R
.2	36°25.8'	33°56.8'	1000	—	0.8	2	3.4		R
.3	36°25.5'	33°57.2'	1000	—	0.4	1	3.3		R
.4	36°25.0'	33°57.6'	1020	—	0.5	2	0.5		R
69.1	36°23.9'	33°58.1'	1050	—	0.6	2	≥1.8		R
72.1	36°24.3'	33°58.5'	975	4.28	0.4	1	1.4		R
.2	36°24.1'	33°58.7'	950	—	0.4	2	0.0		R
.3	36°24.4'	33°59.1'	950	4.34	0.8	2	1.8		R
.4	36°24.5'	33°59.8'	875	4.65	0.4	1	11.9		R
.6	36°24.1'	34°01.1'	775	—	0.4	1	0.0		R
.8	36°23.8'	34°02.0'	750	—	0.4	1	10.1		R

TABLE IV CAPTION

T is bottom water temperature (°C)

P is the estimated penetration (m) of lowermost probe used for the temperature gradient measurements

N is number of thermistors used for sediment temperature gradient measurements

Q is heat flow in 10^{-6} cal/cm^2-sec using an assumed thermal conductivity of 2.2×10^{-3} cal/cm-°C

NAV is the method of navigation used to determine the station position: D - station position determined using whatever information available; S - the ship was navigated within the acoustic transponder net and the station position is estimated from an empirical expression; A - station position is determined within the acoustic net by an acoustic relay-transponder near the end of the hoisting cable; R - the ship is navigated relative to a taut moored radar transponder and the station position is estimated from an empirical expression.

Figure 18. Bathymetry and heat flow (HFU) in Fracture Zone "B" survey area. Depths are in uncorrected fathoms at a 50 fathom contour interval. The dashed line shows the location of the heat flow and topographic profile given in Figure 19. The circles with the cross in them mark the positions of the three acoustic bottom transponders.

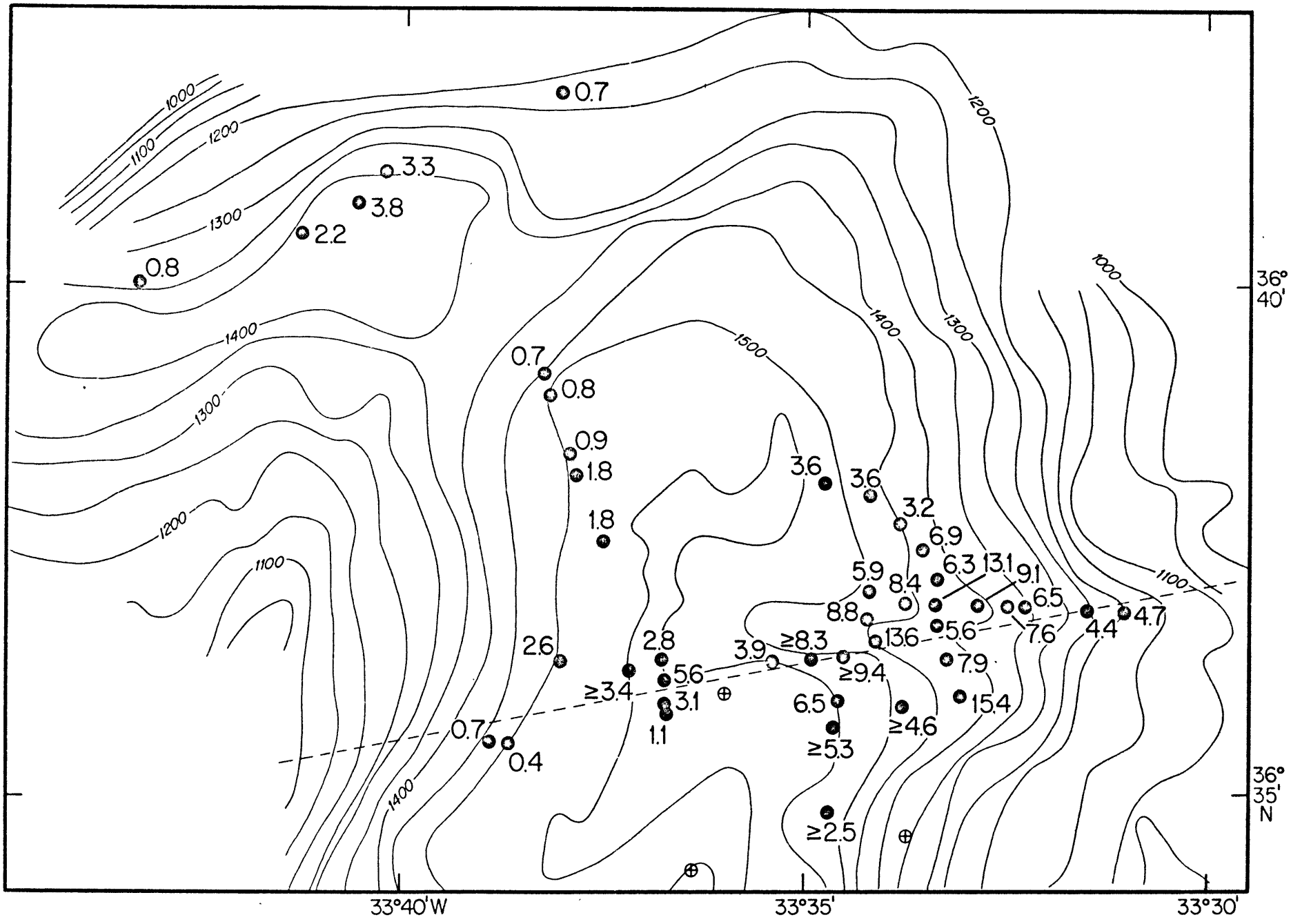
1000
1100
1200
1300
1400
1500
0.7
3.3
3.8
2.2
0.8
0.7
0.8
0.9
1.8
1.8
2.6
0.7
0.4
3.6
3.6
3.2
6.9
5.9
8.4
6.3
13.1
9.1
6.5
8.8
5.6
7.6
4.4
4.7
13.6
2.8
3.9
≥8.3
≥9.4
7.9
5.6
≥3.4
3.1
1.1
6.5
15.4
≥4.6
≥5.3
≥2.5
36° 40'
36° 35' N
33°40'W
33°35'
33°30'

instruments were utilized. The first was a 2 1/2 m short probe device described by Von Herzen and Anderson (1972). The other was a "POGO" probe that the author designed especially for use in the rugged terrain of the Mid-Atlantic Ridge crest.

The POGO probe used the same heat-flow recorder and acoustic telemetering instruments as the 2 1/2 m short probe. It contained a weighted sediment probe, designed to penetrate 1 meter, which was mounted inside a large pipe frame. Five outrigger type thermistors were mounted on the probe (two at 9 cm from the tip, two at 50 cm from the tip and one at 90 cm from the tip). The pipe frame provided protection for the instruments and was coupled to the probe in such a way that the probe could retract, like a turtle's head, if it encountered material too hard to penetrate. A camera and strobe light were also mounted inside the frame and triggered by a bottom contact switch. These provided valuable photographs which were used in interpreting the data and evaluating the performance of the new device. In general, the POGO probe worked as expected although it seldom achieved a full meter of penetration, and normally penetrated only 60-70% of full penetration.

No thermal conductivity measurements were made in the area. The author calculated an average of Mid-Atlantic Ridge thermal conductivities at 2.2×10^{-3} cal/°C-cm-sec. This value is

assumed for all the stations and results in an uncertainty of ±10% in the heat-flow values. This uncertainty has a negligible effect for the purpose of the discussion that follows.

Large errors can result from limited sediment penetration if significant bottom water temperature changes have occurred, (see for instance, Talwani et al., 1971). The deepest penetration achieved in this study was 2.5 meters. I have seen no evidence for such water temperature variations in the measured sediment thermal gradients. But since deeper penetration was not possible, due to a lack of sufficient sediment thicknesses, more evidence is needed to eliminate this possibility.

It is reasonable to assume that any bottom water temperature change would affect the entire floor of the valley. A rise in the water temperature would yield lower and possibly negative near surface geothermal gradients. Similarly, a lowering of the water temperature should result in uniformly high thermal gradients. The heat-flow measurements in FZ"B" vary from a low value of 0.4 HFU to extremely high values of greater than 15 HFU. This implies that, even though bottom water temperature changes cannot be completely eliminated, their effect is not sufficient to alter the local pattern of heat flow.

Navigation was accomplished utilizing, whenever possible, a triangular net of 3 acoustic bottom transponders. On 30 of the heat-flow stations the instrumentation was navigated inside the transponder net with near bottom acoustic equipment (relay transponder) attached to the hoisting cable; the positioning had an accuracy of approximately ±200 meters relative to the bathymetry (Fig. 9). On an additional 8 stations it was only possible to navigate the ship acoustically. The position of the heat-flow measurement was determined from an empirical relation between the wire angle and the horizontal distance to the relay transponder, developed on stations where relay transponder navigation was available. The author estimates the uncertainty of station positions determined by this method at ±400 meters. No acoustic navigation positions were available on the remaining 5 stations. These stations were located by a combination of satellite navigation, bathymetry, ranges to a single bottom transponder and dead reckoning. The quality of these positions varies but on the average is no better than ±1 km.

B. 3. Interpretation and Discussion

A systematic heat-flow pattern is clearly visible in Figures 18 and 19. On the western side of the depression the conductive heat flow is low. Near the eastern side there is a

Figure 19. Heat-flow data and topography in Fracture Zone "B" along the profile shown by the dashed line in Figure 18. The heat flow values illustrated are within two kilometers of the profile line. Stations more than two kilometers from the line are not plotted. Closed circles are the actual value and triangles are minimum values. The solid lines connects averages of measured heat flow values and the vertical bars are ± two standard errors.

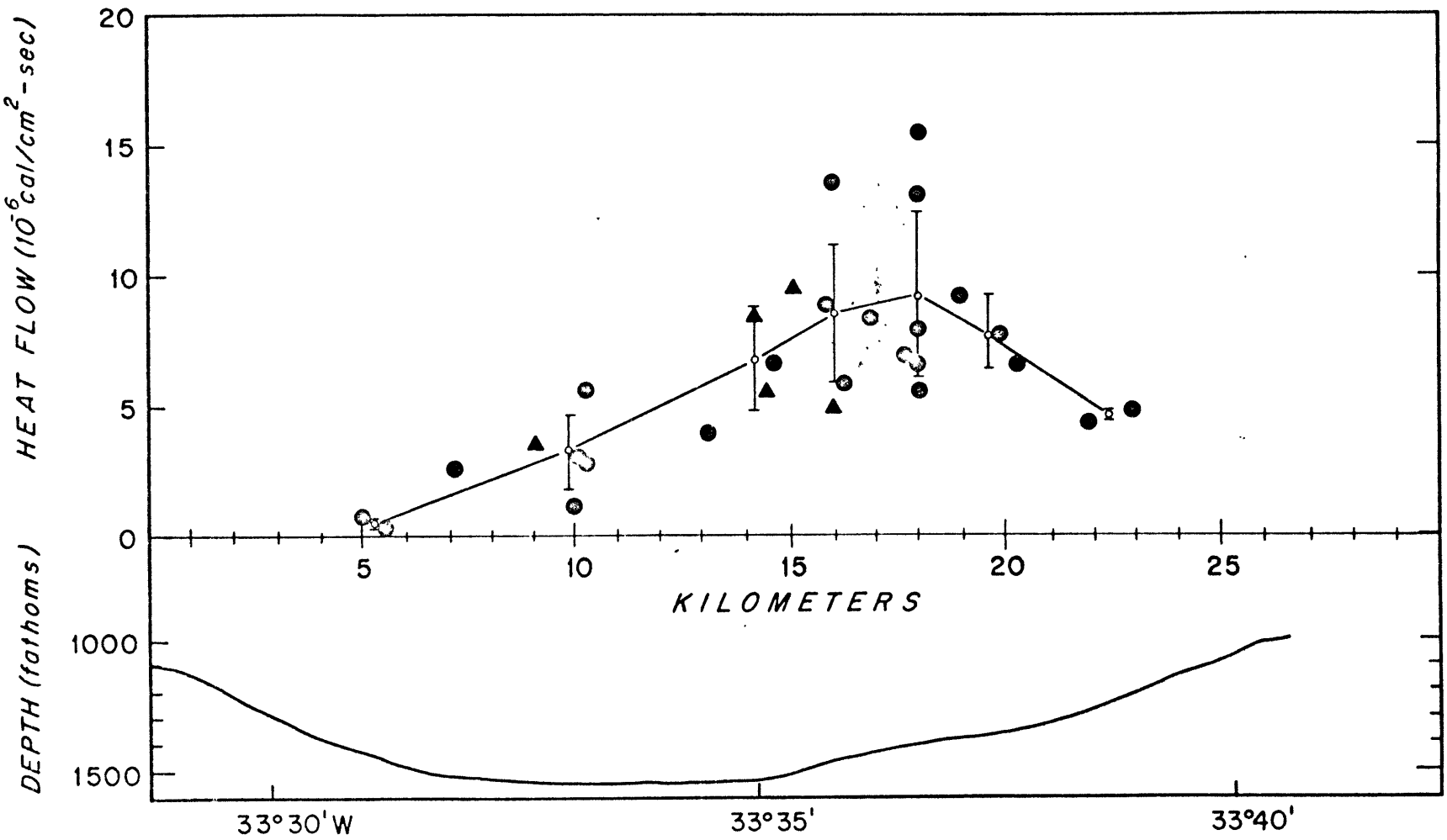
HEAT FLOW (10^{-6}cal/cm^2-sec)
20
15
10
5
0
5
10
15
20
25
KILOMETERS
DEPTH (fathoms)
1000
1500
33°30'W
33°35'
33°40'

prominent conductive heat flow high. Heat flow apparently decreases to the west, north, and east of this high. What happens to the south is not clear. There are other gaps in the data in which additional areas of low or high heat flow may be hidden.

This is not a simple pattern to interpret. Again, the presence of such low heat flow values strongly suggests hydrothermal circulation. Some of them are located near the bottom of the western scarp, but because no significant sediment thicknesses were observed it seeems unlikely that these low values are a result of sediment slumping or thermal refraction.

It is difficult to predict what heat flow values should be expected in this region. The age of crust probably varies from extremely young in the southwest portion, where the spreading center enters the depression, to ages of 2 to 3 m.y. in the northeast section across the fracture where the crust belongs to a different crustal block. Because the precise location and nature of the fracture are unknown it is not possible to determine where and how rapidly this transition occurs. Regardless, the measured heat flow is still substantially less than that predicted by theoretical conductive cooling models.

The profile shown in Figure 19 has a wavelength of about 16 km. This seems to be too high for any reasonable convective system unless it penetrates more than 9 km below the sea floor. Of course, if this profile is at a shallow angle to the axis of a two-dimensional roll, the actual wavelength of the motion could be much less. The data suggests a smaller north-south wavelength but the data coverage is not sufficient to be conclusive.

Since the circulation pattern is unclear, the mechanisms that control it are likewise unclear. There is no apparent correlation with topography. Some form of cellular convection is possible, but if this is the case it is probably related to a variation in the strength of the heat source. Another plausible explanation is a system that has widely scattered discrete zones of high permeability (Bodvarsson and Lowell, 1973). Such a system could take many forms but is still limited by a length to height ratio near 1.

The source of the heat-flow pattern may not be well defined but a definite and systematic variation does exist. In both the Galapagos Spreading Center and here, it has been possible to make enough measurements, and the seemingly confused scatter of spreading ridge heat-flow data has been shown

to be systematic. In both cases, the scale of the variations is measured in kilometers which is indicative of the depth of the hydrothermal circulation.

C. Western Rift Mountains

C. 1. Description of area

This study area is located in the western rift mountains southwest of the fracture zone "B" study area (Figs. 17 and 20). These mountains are very rugged with well over 1 km of vertical relief. Depths vary from less than 500 meters to over 1900 meters. The topography is characteristic of block faulting with the trend parallel to the spreading axis. The sediment distribution is extremely variable. In general, topographic lows are sedimented and highs are barren.

C. 2. Measurements and technique

Seventeen of the new measurements reported in Table IV were obtained in the western rift mountains south of fracture zone "B". On an additional nineteen stations no penetration was achieved. Temperature gradients in the sea floor and thermal conductivity were obtained by the same means as described in section B.2 of this chapter.

Figure 20. Bathymetry and heat flow (HFU) in the western rift mountain survey area. Depths are in uncorrected fathoms at a 50 fathom contour interval. The dashed line shows the location of the heat flow and topographic profile given in Figure 21.

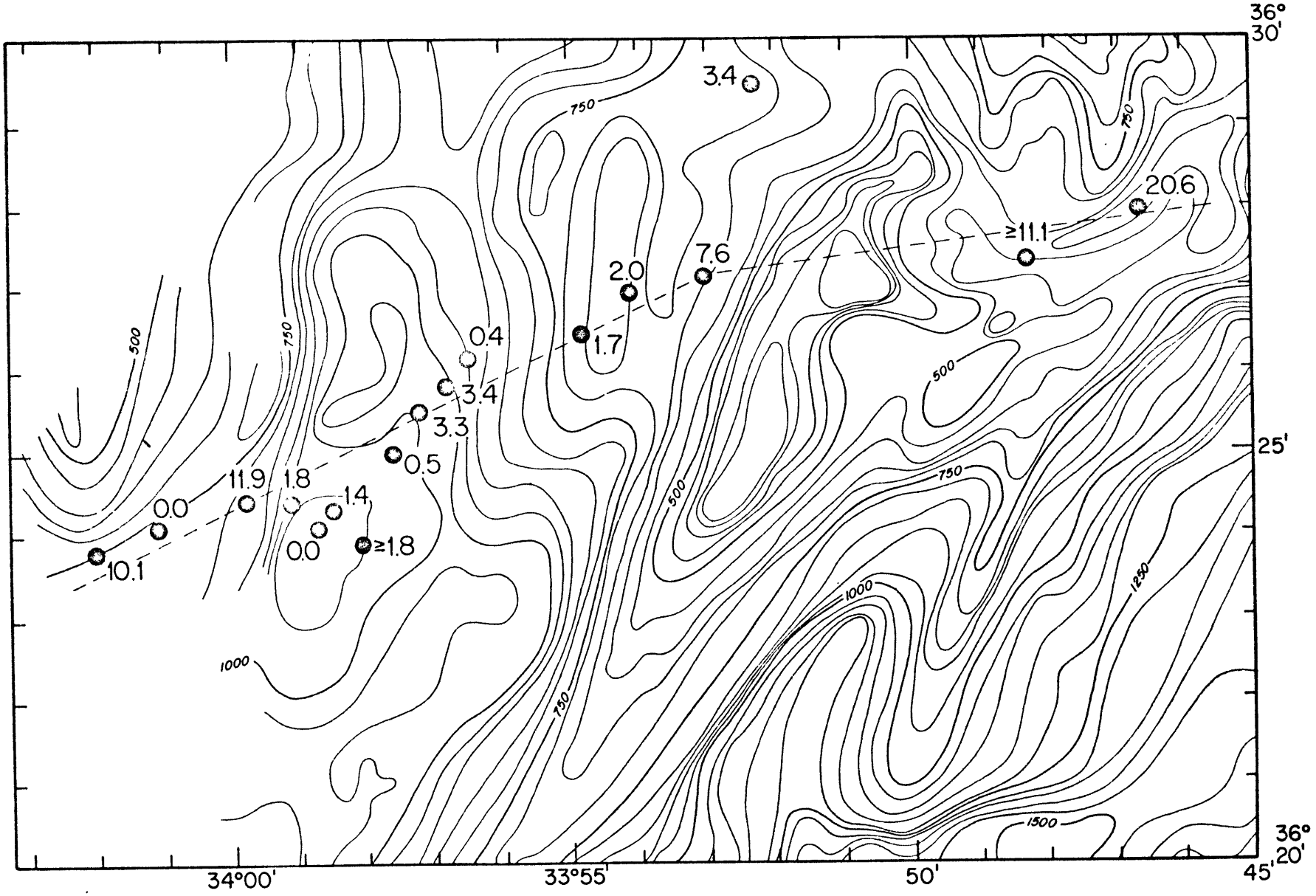
36° 30'
25'
36° 20'
34°00'
33°55'
50'
45'
3.4
750
750
20.6
≥11.1
7.6
2.0
1.7
0.4
3.4
3.3
0.5
500
500
500
750
750
11.9
1.8
1.4
0.0
0.0
≥1.8
10.1
1000
1000
1250
1500

Bottom water temperature changes cannot be ruled out here as easily as in fracture zone"B". I found the water temperatures measured by Fuglister (1960) in general agreement with those I observed, but I was not able to measure depth accurately. Again, because heat-flow values vary over a wide range between depths 1000 and 1900 meters, a large increase or decrease in the bottom water temperatures seems unlikely. This argument is not valid on the stations above 1000 meters (Sta. 60.1 and 60.4).

Navigation was accomplished utilizing a tautly moored radar transponder. Positions relative to the transponder were determined by radar ranges and bearings to this single transponder. The position of the transponder was determined by resolving multiple sateillite fixes while within range of the transponder. The ship positions are probably accurate to ±300 m and the station positions, relative to the ship, are good to ±300 m. Therefore for the uncertainty of the station positions should be less than ±500 m.

C. 3. Interpretation

The first observation to be made from the 25 km long profile shown in Figure 21 is that it displays the same characteristics commonly observed on active spreading centers, i.e. lower heat flow than predicted by theoretical conductive cooling models

Figure 21. Heat-flow data and topography in the western rift mountains along the profile shown by the dashed line in Figure 20. Closed circles are the actual value and triangles are minimum values. The dashed line is the theoretical heat flow (see Figure 6).

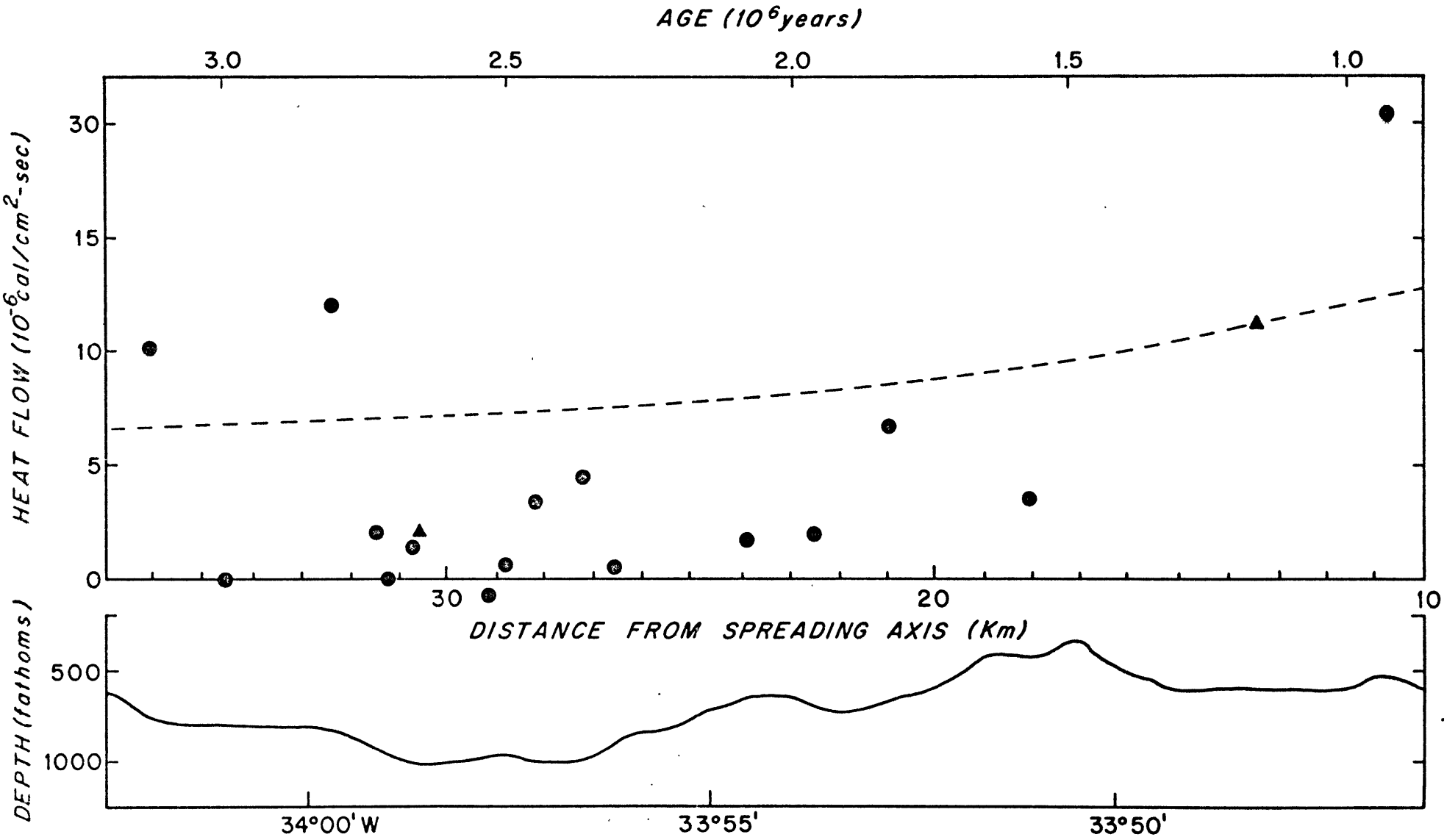
AGE (10^6 years)
3.0
2.5
2.0
1.5
1.0
HEAT FLOW (10^{-6} cal/cm^2-sec)
30
15
10
5
0
30
20
10
DISTANCE FROM SPREADING AXIS (Km)
DEPTH (fathoms)
500
1000
34°00' W
33°55'
33°50'

with a large scatter in the individual measurements . I have approximately one successful measurement for each two kilometers of profile. This is not high enough density of measurements to clearly discern a modulation wavelength like the 6 km wavelength found on the Galapagos Spreading Center. Nevertheless, the similarity is inescapable; the values observed on this profile fit nicely to a 5 to 6 km wavelength. However, there is very little correlation between topography and heat flow.

It is unlikely that all the low values and the scatter are caused by environmental effects such as sediment slumping, or that the obvious discrepancy between observed and predicted heat (Fig. 21) is not significant. Therefore, I conclude that the crust in this region contains an active hydrothermal system. As I discuss in Chapter III, with such high amplitude topography there is no reason to assume the convection must be cellular in nature.

It is an unfortunate fact that existing technology does not allow more measurements in such a sparsely sedimented area. As a result this rift mountain survey fails to reveal a convincing pattern and does not add much to our knowledge of heat loss from an active oceanic ridge.

D. Conclusion

The primary purpose of this Mid-Atlantic Ridge heat-flow study was to provide a basis of comparison for the Galapagos Spreading Center data. This endeavor achieved limited success. As on the Galapagos Spreading Center,both the rift mountain area and fracture zone "B" had an average heat flow well below the theoretical, predicted value. In addition, extremely low heat-flow values were observed. These low values, much lower than is observed on the Earth's oldest and most stable crust, are apparently located near descending limbs of a hydrothermal cell.

A systematic variation in the heat-flow pattern was clear in fracture zone "B". The wavelength of this pattern is at least several kilometers which is comparable to the Galapagos Spreading Center and implies deep penetrating circulation. A similar situation is suggested in the western rift mountain area but there is not a high enough density of data to make a definitive judgement.

The fracture zone "B" hydrothermal system is three-dimensional in nature,with the E-W axis apparently substantially larger than the N-S axis.

In summary, the existence of extensive deep penetrating hydrothermal circulation is implied by this data and to this

extent this study provides a useful basis of comparison for the Galapagos Spreading Center. However, the nature of the hydrothermal systems on the Mid-Atlantic Ridge is somewhat more obscure. Hopefully some of the other geophysical and geological data obtained in this region including additional thermal data will yield a better understanding of the hydrothermal systems.

CHAPTER VI

SUMMARY

Lithospheric cooling along the Galapagos Spreading Center at 86°W longitude, as determined by surface heat-flow measurements, appears dominated by hydrothermal circulation. This same phenomena apparently exists on the Mid-Atlantic Ridge at 36°N and presumably, in some form, on all active oceanic ridges. It is responsible for removing the majority of the heat (> 80%) lost through young (few m.y. old) crust. This component of heat has been ignored in previous calculations of the total rate of heat loss by the Earth.

A theoretical expression is used to estimate the heat released by sea-floor spreading, since current technology does not provide any means for direct measurement. The revised value of 10.2×10^{12} cal/sec (±15%) represents a 32% increase over previous estimates. More than 20% of this heat apparently escapes through hydrothermal vents near sea-floor spreading centers. The previously accepted equality of oceanic and continental heat flux is invalid. The revised analysis indicates the oceanic heat flux is 2.2 HFU versus 1.5 for the continents. The average for the Earth is then approximately 2.0 HFU.

The horizontal wavelength of inferred hydrothermal convection at the Galapagos Spreading Center, in the one dimension measured, is 6 ±1 km. The systematic modulation suggests cellular convection. If the system is dominated by cellular convection, the depth of penetration, based on laboratory modeling experiments should be 3 to 4 kilometers.

The data from the Galapagos Spreading Center and laboratory experiments both suggest that the position of the cells in a cellular convection system can be a strong function of the local topography, the rising limbs of flow being located beneath topographic highs and the descending limbs beneath topographic lows. The addition of topography also enhances the heat transfer efficiency of a convection system. Lateral variation in permeability or the systems bottom boundary condition will also influence the position of cells. Even if the circulation system were strongly influenced by some combination of variations in the strength of the heat source, topography or discrete zones of high permeability, it would probably still be cellular in nature, and similar deep penetration is indicated.

If the Galapagos Spreading Center is typical, there are presumably numerous hydrothermal springs and fissures in each square kilometer of near-ridge sea floor and the sediments of

thicknesses of at least 50 meters are apparently penetrable to fluid flow. As the sea floor ages the surface of the hydrothermal system becomes less permeable and eventually both the surface and the deep system are completely clogged and sealed. The age at which this occurs varies from ridge to ridge but there is evidence that suggests it may not be complete until the crust is at least 8 m.y. old (Sclater et al., in press) and possibly as much as 40-50 m.y. old (Williams and Poehls, in preparation). Most of the surface is apparently sealed long before hydrothermal circulation stops, although some vents do persist. This sequence is probably responsible for the heat-flow patterns shown in Figure 1. The axis minima would result from unhindered hydrothermal cooling and the observations are additionally biased low by locating heat-flow stations in sediment ponds. The first maxima occurs when the surface becomes nearly sealed by sediment forcing the heat to be conducted through this boundary. Also these station positions are less influenced by sediment distribution. The second minima could be derived from a combination of effects (e.g. decreasing total heat flow, mineralogical phase changes, and continued hydrothermal heat loss) but this is speculation based on a limited study. After this the observed heat flow presumably reaches a value more representative of the actual, undistrubed total heat flow.

The results of this study show the difficulties in resolving systematic patterns in the heat-flow distribution on spreading ridges. Numerous, closely-spaced measurements with precise navigation combined with a relatively uniform sediment cover, appear to be necessary ingredients for recognition of the heat-flow pattern.

The rate of energy release through hydrothermal circulation near active ocean ridges is somewhat greater than man's rate of energy consumption. But the logistics, the hostile sea-floor environment and the fact that the heat loss is spread over millions of square kilometers of sea floor makes its economic value questionable except on shallow, near-shore or subareal spreading centers such as the Reykjanes Peninsula.

The results of this study indicate several avenues for future work. Revisiting the Galapagos Spreading Center at 86°W longitude would permit a study of the three-dimensionality of the convection systems. Other geophysical and geological techniques could be applied; core samples might be obtained from the sediment mounds and possibly hot springs could be located, mapped and sampled. Where conditions permit,other active spreading ridges should be surveyed. This ideally should be done on ridge segments similar to the Galapagos Spreading Center study and ridge segments with different spreading rates and morphology. Laboratory studies should be continued with emphasis on studying

the effects of variations in upper and lower boundary conditions (e.g. free discharge, topography and variable heat source strengths) and the interior parameters (e.g. permeability). With this type of data it should be possible to gain a considerably better understanding of hydrothermal circulation in the oceanic crust.

APPENDIX I. Hele-Shaw Apparatus

The cell is fabricated from clear acrylic plastic. ($K \approx 4.5 \times 10^{-3}$ cal/cm-sec-°C). The upper boundary is a copper pipe, through isothermal water was pumped at a high flow rate from a constant temperature bath (Fig. A1). The lower boundary is modeled by insulated resistance wire submerged in mercury. The temperature difference (ΔT) is controlled by varying the bath temperature and the electrical current through the resistance wire. The lower boundary more closely resembles a constant heat flow than a constant temperature. The boundary condition in an actual hydrothermal system is of course unknown but the change to a constant heat flow boundary is reasonable.

The cavity of width a between two sheets of acrylic is filled with a viscous silicone oil (Dow Corning 200 Fluid). To allow the flow to be visualized, very fine aluminum particles are suspended in the fluid and the outside of one wall of the cavity was covered with an opaque black material (e.g. paint on paper). The aluminum particles tend to align themselves with the fluid shear therefore becoming less visible in regions of rapid flow. Temperatures are monitored by thermistors mounted in the bath and mercury. The entire cell is insulated with 3 to 6 inches of styrofoam to reduce heat loss to the room and

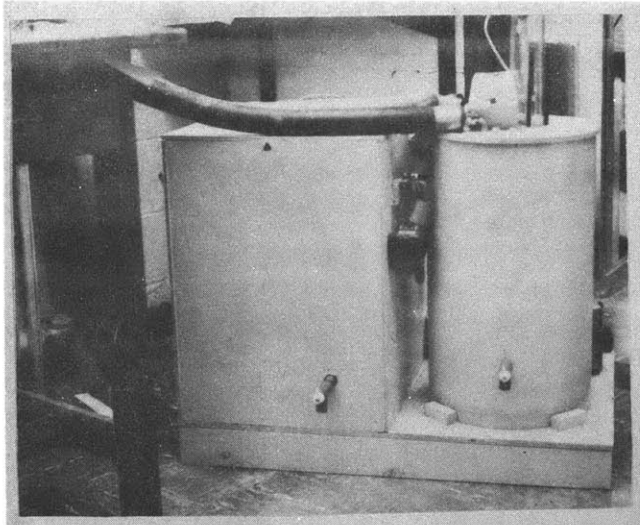

Front View of Temperature Bath

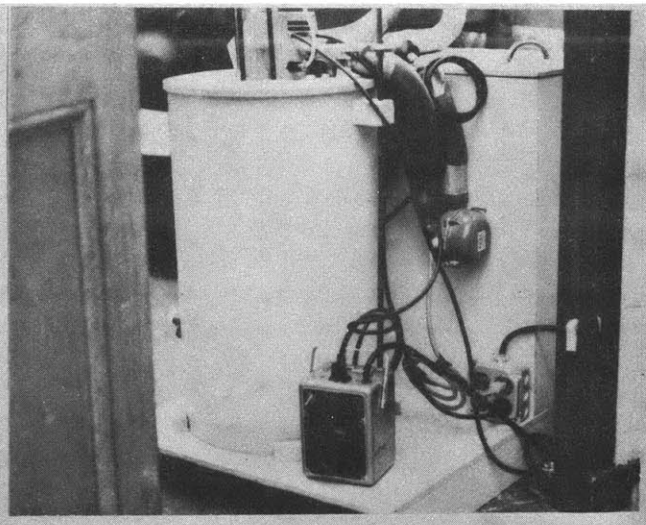

Rear View of Temperature Bath

Top View of Temperature Bath

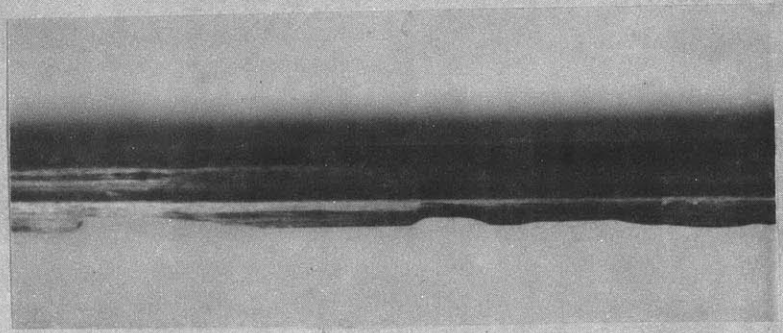

Upper Boundary Copper Pipe with Topography

Figure A1

the effects of variations in room temperature. The insulation has to be removed only briefly to allow photographing the cell (Fig. A2).

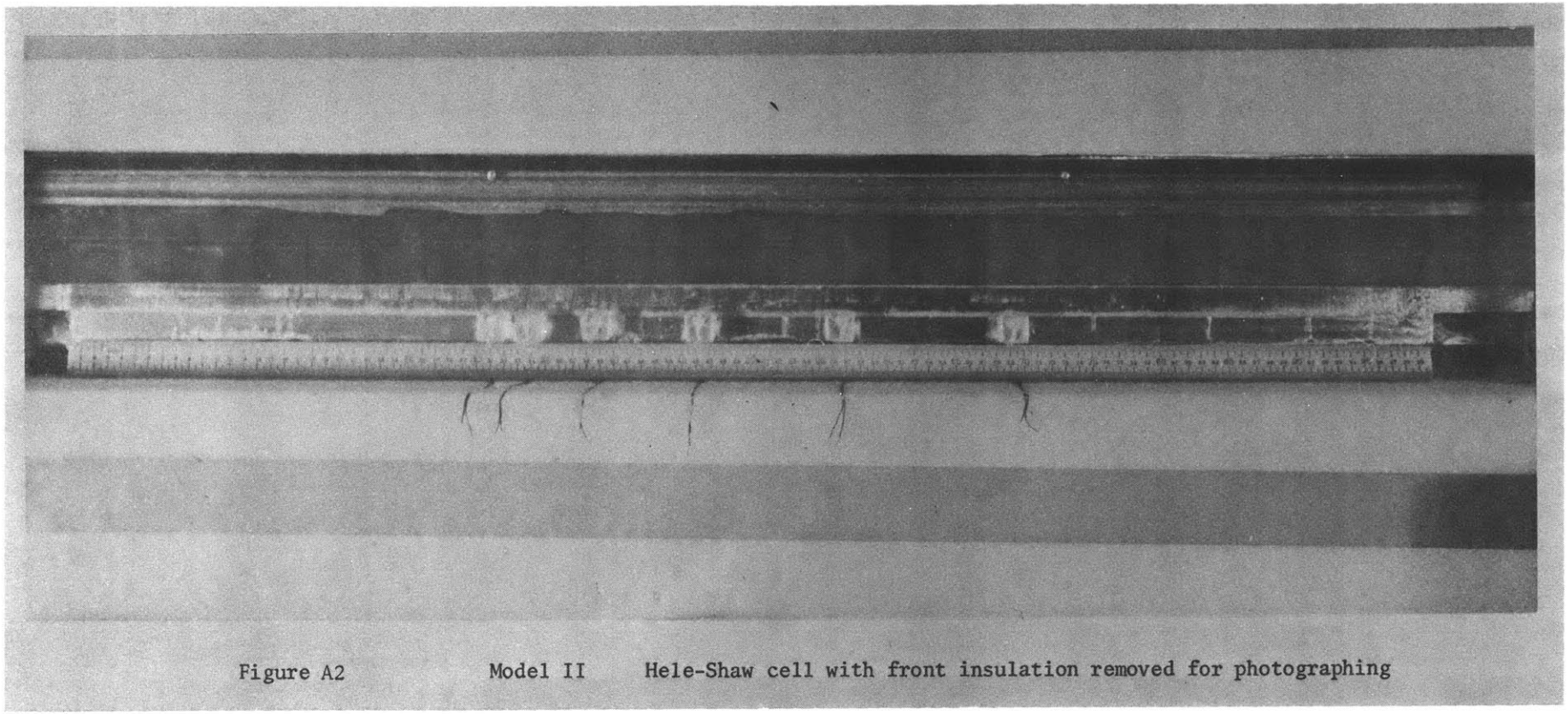

Figure A2 Model II Hele-Shaw cell with front insulation removed for photographing

REFERENCES

Anderson, R.N., 1972, Low heat flow on flanks of slow spreading mid-ocean ridges, Geol. Soc. Am. Bull., 83, 1947.

Aumento, F., Loncarevic, B.D. and Ross, D.I., 1971, Hudson geotraverse: geology of the Mid-Atlantic Ridge at 45'N, Phil. Trans. Roy. Soc. Lond. A., 268, 623.

Batchelor, G.K., 1954, Heat convection and buoyancy effects in fluids, Meteoral. Soc., 80, 339.

Bodvarsson, G., 1961, Physical characteristic of natural heat resources in Iceland, Jökull, 7, 29.

Bodvarrson, G. and Lowell, R.P., 1972, Ocean-floor heat flow and the circulation of interstitial waters, J. Geophys. Res., 77, 4472.

Boegeman, D.E., and Miller, G.S., 1972, Precise positioning for near bottom equipment using a relay transponder, Mar. Geophys. Res., 7, 381.

Bullard, E.C., Maxwell, A.E., and Revelle, R., 1956, Heat flow through the deep sea floor, Adv. Geophys. 3, 153.

Corliss, J.B., 1971, The origin of metal-bearing submarine hydrothermal solutions, J. Geophys. Res., 76, 8128.

Corry, C., Dubois, C. and Vacquier, V., 1968, Instrument for measuring terrestrial heat flow through the ocean floor, J. Marine Res., 26, 165.

Darcy, H.P.G., 1856, Les fontaines publiques de la ville de Dijon, Victor Dalmont, Paris.

Deffeyes, K.S., 1970, The axial valley: a steady state feature of the terrain, in Megatectonics of continents and oceans, New Brunswick, Rutgers U. Press.

Donaldson, I.G., 1962, Temperature gradients in the upper layers of the Earth's crust due to convecture water flows, J. Geophys. Res., 67, 3449.

Elder, J.W., 1965, Physical processes in geothermal areas, Am. Geophys. Un. Mono., 8, 211.

Elder, J.W., 1967, Steady free convection in a porous medium heated from below, J. Fluid Mech., 27, 29.

Erickson, A.J., and Simmons, G., 1969, Thermal measurements in the Red Sea hot brine pools, in Hot brines and recent heavy metal deposits in the Red Sea, ed. by E.T. Degens and D.A. Ross, Springer-Verlag, New York.

Fisher, Robert L., Sclater, John G. and MacKenzie, D.P., 1971, Evolution of the Central Indian Ocean Ridge; Western Indian Ocean, Geol. Soc. Am. Bull., 82, 553.

Forsyth, D.W., and Press, F., 1971, Geophysical tests of petrological models of the spreading lithosphere, J. Geophys. Res., 76, 7963.

Fuglister, F.C., 1960, Atlantic Ocean atlas of temperature and salinity profiles and data from the International Geophysical year of 1957-1958, publ. by Woods Hole Oceanographic Institution, 209 p.

Grim, P.J., 1970, Connection of Panama fracture zone with the Galapagos rift zone, eastern tropical Pacific, Marine Geophys. Res., 1, 85.

Heirtzler, J.R. and Le Pichon, X., in press, A study of the genesis of tectonic plates, Geology.

Hele-Shaw, H.S.J., 1898, Trans. Inst. Naval Architects, 40, 21.

Hendershott, M.C., 1973, Ocean tides, EOS, 54, 76.

Herron, E.M., 1972, Sea-floor spreading and the Cenozoic history of the east-central Pacific, Geol. Soc. Am. Bull., 83, 1671.

Herron, E.M., and Heirtzler, J.R., 1967, Sea-floor spreading near the Galapagos, Science, 158, 775.

Hekinian, R., 1974, Petrology of igneous rocks from Leg 22 in the northwest Indian Ocean, Repts. Deep Sea Drilling Project, 22, Washington, D.C. printing office, 413.

Hey, R.N., Deffeyes, K.S., Johnson, G.L., and Lowrie, A., 1972, The Galapagos triple junction and plate motions in the east Pacific, Nature, 237, 20.

Hyndman, R.D., and Rankin, D.S., 1972, The Mid-Atlantic Ridge near 45°N XVIII: Heat-flow measurements, Can. J. Earth Sci., 9, 664.

Lachenbruch, A.H., 1968, Rapid estimation of the topographic disturbance to superficial thermal gradients, Rev. Geophys. 6, 365.

Lachenbruch, A.H., 1973, A simple mechanical model for oceanic spreading centers, J. Geophys. Res., 78, 3395.

Lamb, H., 1932, Hydrodynamics, Cambridge University Press, London.

Langseth, M.G., Le Pichon, X , and Ewing, M., 1966, Crustal structure of mid-ocean ridges. 5. Heat flow through the Atlantic Ocean floor and convection currents, J. Geophys. Res., 71, 5321.

Langseth,M.G. and Von Herzen, R.P., 1971, Heat flow through the floor of the world oceans, in The Sea, V. 4, Part 1, ed. by A.E. Maxwell, Wiley-Interscience, 299.

Lapwood, E.R., 1948, Convection of a fluid in a porous medium, Proc. Camb. Phil. Soc., 44, 508.

Larson, R.L. and Chase, C.G., 1972, Late Mesozoic Evolution of the Western Pacific Ocean, Geol. Soc. Am. Bull., 83, 3627.

Larson, Roger L. and Pitman, W.C., World-wide correlation of Mesozoic magnetic anomalies, and its implications, Geol. Soc. Am. Bull., 83, 3645.

Lee, W.H.K., 1970, On the global variations of terrestrial heat flow, Phys. Earth Planet. Int., 2, 332.

Lee, W.H.K. and Uyeda, S., 1965, Review of heat flow data, Am. Geophys. Un., Geophys. Mono., 8, 87.

Le Pichon, X., and Langseth, M.G., 1969, Heat flow from mid-ocean ridges and sea-floor spreading, Tectonophys., 8, 319.

Lister, C.R.B., 1970, Heat flow west of the Juan de Fuca Ridge, J. Geophys. Res., 75, 2648.

Lister, C.R.B., 1972, On the thermal balance of a mid-ocean ridge, Geophys. J.R. astr. Soc., 26, 515.

McKenzie, D.P., 1967, Some remarks on heat flow and gravity anomalies, J. Geophys. Res., 72, 6261

McKenzie, D.P., 1968, The influence of the boundary conditions and rotation on convection in the Earth's mantle, Geophys. J. Roy. Ast. Soc. 15, 457.

McKenzie, D.P., and Sclater, J.G., 1969, Heat flow in the eastern Pacific and sea-floor spreading, Bull. Volcanol., 33-1, 101.

McNitt, J.R., 1965, Review of geothermal resources, Am. Geophys. Un. Mono., 9, 240.

Menard, H.W., and Smith, S.M., 1966, Hypsometry of ocean basin provinces, J. Geophys. Res., 71, 4305.

Nishimori, R.K. and Anderson, R.N., Gabbro, serpentinite, and mafic breccia from the East Pacific, in press, Earth Planet. Sci. Lett.

Miyashiro, A., Shido, F., and Ewing, M., 1971, Metamorphism in the Mid-Atlantic Ridge near 24° and 30°N, Phil. Trans. Roy. Soc. Lond. A., 268, 589.

Palmason, G., 1967, On heat flow in Iceland in relation to the Mid-Atlantic Ridge, Visindafjelay Islendinaga, Ret. 1967 Rep. of a symposium, Geoscience Soc., Iceland, Reykjavik, 111.

Parker, R.L., and Oldenburg, D.W., 1973, Thermal model of ocean ridges, Nature, 242, 137.

Preisinger, A., 1965, Prehnite — ein Schichtsilikatty, Tschermaks Mineral Petrg. Mitt., 10, 491.

Raff, A.D., 1968, Sea-floor spreading: Another rift, J. Geophys. Res., 73, 3699.

Reid, I. and Macdonald, K., 1973, Microearthquake study of the Mid-Atlantic Ridge near 37°N, using sonobuoys, Nature, 246, 88.

Robie, R.A., Bethke, P.M., Toulmin, M.S., and Edwards, J.L., 1966, X-ray crystallographic data, densities, and molar volumes of minerals: Geol. Soc. Am. Bull., Mem. 97, 27.

Rouse, H., Yih, C-S, and Humphreys, H.W., 1952, Gravitational convection from a boundary source, Tellus, 4, 201.

Sayles, F.L., and Bischoff, J.L., 1973, Ferromagnaoan sediments in the equatorial East Pacific, Earth & Planet. Sci. Lett., 19, 330.

Schatz, J.F., and Simmons, G., 1972, Thermal conductivity of Earth materials at high temperatures, J. Geophys. Res., 77, 6966.

Sclater, J.G., and Francheteau, J., 1970, The implications of terrestrial heat flow observations on current tectonic and geochemical models of the crust and upper mantle of the Earth, Geophys. J. R. astr. Soc., 20, 509.

Sclater, J.G., and Harrison, C.G.A., 1971, Elevation of the Southwest Indian Ridge, Nature, 230, 175.

Sclater, J.G., and Klitgord, K.D., 1973, A detailed heat flow, topographic and magnetic survey across the Galapagos Spreading Center at 86°W, J. Geophys. Res., 78, 6951.

Sclater, J.G., Von Herzen, R.P., Williams, D. L., Anderson, R.N. and Klitgord, K., in press, The heat flow low on the flank of the Galapagos Spreading Center, Geophys. J. Roy. astr. Soc.

Sleep, N.H., 1969, Sensitivity of heat flow and gravity to the mechanism of sea-floor spreading, J. Geophys. Res., 72, 542.

Spooner, E.T.C. and Fyfe, W.S., 1973, Sub-sea-floor metamorphism, heat and mass transfer, Contr. Mineral. and Petrol. 42, 287.

Steinfink, H., 1958, The crystal structure of Chlorite. II. A triclinic polymorph: Acta Cryst., 11, 195.

_____ , 1961, Accuracy in structure analysis of layer silicates: Some further comments on the structure of prochlorite: Acta Cryst., 14, 198.

_____ , 1962, A correction — the crystal structure of Chlorite. I. A monoclinic polymorph: Acta Cryst, 15, 1310.

Talwani, M., Windisch, C.C., and Langseth, M.G., 1971, Reykjanes ridge crest: a detailed geophysical study, J. Geophys. Res., 76, 473.

Turner, J.S., 1969, Buoyant plumes and thermals, Ann. Rev. Fluid Mech., 1, 29.

van Andel, T.H., and Heath, G.R., 1973, Initial reports of the Deep Sea Drilling Project, Vol. 16, Washington, D. C. (U.S. Government Printing Office).

van Andel, T.H., Heath, G.R., Malfait, B.T., Heinrichs, D.F., and Ewing, J.L., 1971, Tectonics of the Panama basin, eastern equatorial Pacific, Geol. Soc. Am. Bull., 82, 1489.

Veevers, J.J., and Heritzler, J.R., 1973, Deep Sea Drilling Project Leg 27, Geotimes, 18, 4.

Verhoogen, J., 1973, Possible temperatures in the oceanic upper mantle and the formation of magma, Geol. Soc. Amer. Bull. 84, 515.

Von Herzen, R.P., and Maxwell, A.E., 1959, The measurement of thermal conductivity of deep sea sediments by a needle-probe method, J. Geophys. Res., 64, 1557.

Von Herzen, R.P., and Anderson, R.N., 1972, Implications of heat flow and bottom water temperature in the eastern equatorial Pacific, Geophys. J.R. astr. Soc., 26, 427.

Von Herzen, R.P., and Langseth, M.G., 1966, Present status of oceanic heat flow measurements, Phys. Chem. Earth, 6, 365.

Von Herzen, R.P., and Uyeda, S., 1963, Heat flow through the eastern Pacific Ocean floor, J. Geophys. Res., 67, 4219.

Von Herzen, R.P. and Vacquier, V., 1966, Heat flow and magnetic profiles on the Mid-Indian Ocean Ridge, Phil. Trans. Roy. Soc. Lond., A, 259, 262.

Williams, D.L., and Poehls, K., in preparation, Thermal modeling of the oceanic lithosphere.

Wooding, R.A., 1960, Instability of a viscous liquid of variable density in a vertical Hele-Shaw cell, J. Fluid Mech., 7, 501.